Electronic Theses and Dissertations

2017

Development of Highly Sensitive and Selective Breathing Sensors Using Molecular Imprinted Filtering for Diabetic and Alcoholic Patients

Md. Saleh Akram Bhuiyan
South Dakota State University

DEVELOPMENT OF HIGHLY SENSITIVE AND SELECTIVE BREATHING

SENSORS USING MOLECULAR IMPRINTED FILTERING FOR DIABETIC AND

ALCOHOLIC PATIENTS

BY

MD. SALEH AKRAM BHUIYAN

A thesis submitted in partial contentment of the requirements for the

Master of Science

Major in Electrical Engineering

South Dakota State University

2017

DEVELOPMENT OF HIGHLY SENSITIVE AND SELECTIVE BREATHING SENSORS USING MOLECULAR IMPRINTED FILTERING FOR DIABETIC AND ALCOHOLIC PATIENTS

This thesis is authorized as a praiseworthy and self-contained research by an aspirant for the Master of Science degree in Electrical Engineering and is satisfactory for meeting all the thesis qualifying requirements for this degree. The approval of this thesis work does not infer that the closures stretched by the aspirant are certainly the closures of the major department.

Qiquan Qiao, Ph.D.   Date
Thesis Advisor

Steven Hietpas, Ph.D.   Date
Head, Department of Electrical
Engineering and Computer Science

Dean, Graduate School   Date

ACKNOWLEDGEMENTS

My profound gratitude goes foremost to my thesis and research supervisor Dr. Qiquan Qiao for giving me the prospect to work as a graduate research assistant in his excellent research center and for his immense inspiration, supports and technical supervision during the research phase. Dr. Qiao's enthusiasms and suggestions have been imperative in refining the superiority of this thesis.

My appreciation also extends to my thesis committee members, for their valuable time and cordial consideration on reviewing my thesis work. Moreover, I would like to direct my pleasant gratefulness to my research group adherents for their guide and help.

Above ground, I would like to acknowledge my God, Family and Friends for their love and support.

TABLE OF CONTENTS

LIST OF FIGURES

LIST OF TABLES

ABSTRACT

DEVELOPMENT OF HIGHLY SENSITIVE AND SELECTIVE BREATHING
SENSORS USING MOLECULAR IMPRINTED FILTERING FOR DIABETIC AND
ALCOHOLIC PATIENTS

MD. SALEH AKRAM BHUIYAN

2017

Wellness sensor technology is an emerging diagnostic test research field, which mostly deal with the point of care of the patients in the recent days. Due to the lack of awareness from the patients, most diseases cannot be detected in due time. This led to worse conditions, such as diabetic and alcoholic syndrome. Therefore, many research groups have been working to develop portable sensor devices that can track serious diseases. These include diabetic and alcoholic biomarkers in breathing. These devices have very high selectivity and reliability. However, the major limitation of biomarkers is that it deals with the bio-molecular based sensing mechanism. Extensive challenges exist in the selectivity and reliability of breathing sensors. These require development of proper materials and effective detection methods. Thus, selection of proper materials, correct sensing parameters, effective device architecture and simple fabrication processing are substantially critical.

The goal of this work is to develop graphene based breathing sensors with high selectivity and sensitivity using a novel molecular imprinted filtering technique. The sensors have various applications including Point of Care Testing (POCT) device for personalized home and clinical use in early detection of diabetic and alcoholic patients. Different fabrication procedures were used to optimize the sensor performance. The optimized results demonstrate that a proper

xi

biomarker molecule imprinting process could selectively detect diabetes and alcohol. The graphene layer was optimized by maintaining spray coating time, pattern and distance between the substrate and spray coater. Graphene adhesion to the substrate was also improved using polyvinyl pyrrolidone. The molecular imprinting filter made on top of the graphene layer improved the performance of acetone and ethanol molecule detection, indicated by the change of resistance in the graphene layer. The sensors showed poor performance for long-time exposure (> 10 second) due to ambient molecules and moisture. However, the sensor characteristics were significantly improved for short exposing time (3-4 second) due to the optimization in the thickness of the filtering layer and sensing layer.

Chapter 1: Introduction

1.1 Background

The historical diagnostic patterns or systems for diabetes and alcoholic patients are mostly restricted to the medical, research or diagnostic laboratory based disease analysis and prediction schemes. This require transportation of specimens from the patients to the diesease analysis lab in order to find out the disease. This process causes inconvenience. In addition, there are some diseases that cannot be easily detected, if the patients are not aware about them, such as high blood pressure or alcoholism. Thus, portable, efficient, reliable point of care/bedside testing (POCT) devices have entered into the region of the time-consuming laboratory processes, especially in diabetes and alcohol detection. This inspires the development of breathing monitoring based technology.

For diabetic patients, the scarcity of functioning insulin in their blood cells triggers the body to burn fat cells into energy. The disintegrated products of that incident are known as ketones, which can amass in the blood vessels and urine. One form of ketone, named acetone has a divulging "fruity" aroma. When ketones build up, the individual will have a fruity-acetone breath. This is usually known as "nail polish remover breath." A preeminent level of acetone is a cautionary sign that an individual's insulin level is not below the permissible range. If not medicated appropriately with insulin, the acetone stockpile can turn into diabetic ketoacidosis, which can twist toward diabetic coma. The clinical diabetes care scheme should comprise the guiding principle for tracking ketone/acetone - either by diagnosing blood or by plunging a test band in urine. A diabetic patient usually has 2.7 to 3.7 ppm of acetone breath [13], which is very low in measurement scale. this is one of the major challenges in developing breathing sensors.

Similarly, to diabetes, alcohol intake can also be monitored through breath. Until it is all processed, the alcohol will be all over the body, in the blood, the liver, and even in the brain. If it is in the blood, it will consequently be in the lungs. This is the cause of the alcohol breath that

most people refer as "alcohol smell." The acceptable breath alcohol range is 130-208 ppm [13], which is equivalent to the 0.02%-0.08% blood alcohol concentration (BAC).

There are some challenges in the development of breathing sensors. The major problem is to detect diabetes and alcohol at molecular levels. Various sensors have been developed in the last few decades to detect diseases, including diabetes and alcohol without using blood samples. However, the selectivity is still limited. Most of the commercial diabetes and alcohol sensor are still dealing with the complex lab based diagnosis, such as IR spectroscopy (also used by police department in road to detect alcoholic driver) and impedance analysis (for diabetes detection). Therefore, POCT devices, that provide reliable information about the diabetes and alcohol level in the breathing are a very good catch for the users who want to measure their health conditions more conveniently and quickly.

It is already mentioned that in the breath, the acetone (as a diabetes biomarker) is 2.7-3.7 ppm [13]. The alcoholic patients such as drunk drivers used to have 130-208 ppm [13] of ethanol in their breathing. The part per million (ppm) is a very small unit. Thus, that small ppm amount of acetone or ethanol in breathing is needed to be measured efficiently to make a perfect POCT device.

The alcohol breath was first reported in ancient Greek dynasty. In 1803, Mr. Henry first experimented on the gas absorption of water at different temperature and pressure [14]. Later, in 1835, Liebig conveyed that the oxidation of hydroxy group can be done by acid dichromate ($Cr_2O_2^{-7}$) [15]. After that, Anstie first discovered a tool to detect mouth alcohol using the acid dichromate [16]. In 1910 Cushny used "Henry law" to detect alcohol in blood and breath when he was working on the drug effect on blood and breath [17].

After all, those findings, the first breath alcohol analyzer was developed in E. Bogen's lab in 1927 [18]. Later, in 1927 the measurement of the breath alcohol amount was optimized by

WD Mcnally [19]. The name of that device was breath analyzer, but the device installation area was very big. So, later a portable alcohol analyzer was developed by R.N. Hager named as Harger Drunk-O-Meter [20]. But, it requires more than 2 liters equivalent volume of breath in a balloon and was not able to predict the exact amount of breath alcohol; unless the amount is very high. So, at 1941 Jetter, Moore and Forrester introduced intoximeter that was able to measure the amount of ethanol through a time consuming lab based process [21].

At the same time, photoelectric color change based Alcoholometer (by Greenberg and Keator), portable breathalyzer (by R.F. Borkenstein) and pocket size breath testing device (by Otto Heinrich Drager) was used to measure alcohol breath [22-24], but, these devices are not that much reusable, so, JR penton and MR Forrester developed chromatographic analysis based Breath analyzer which is a very complex device and need high maintenance due to the optical based analysis [25]. After that, during 1972 – 1977 Electrochemical breath analysis [26], IR incorporated with electrochemical analysis, IR-Mass spectroscopy [27] was used to detect breath alcohol and finally Alcyltron (1978), Datamaster,Alcomat and Alcotest (1979) devices were released and being used till 2004. All those systems are focused on the method to detect alcohol not concerned about the amount of alcohol to detect.

At 1552 BC the frequent urination was detected by physician Hes-Ra due to the excessive sugar level in patients' blood. Upto, 11th century it was known as obesity towards sugar or diabetes (diabetes mallitus). From 1800's to 1960's only Benedict solution based method was used to detect diabetes, which was not reusable and needs a lot costs. Though, at 1936 Dr. Himsworth first informed that diabetes can be two types based on insulin levels, Type 1 (insulin-dependent) diabetes and Type 2 (noninsulin-dependent) diabetes. However, the first home testing strips for diabetes was being introduced in 1960, that needs a drop of blood on the strip and the color change of the strip used to indicate blood glucose/sugar level. Later, at 1970 first blood

glucose meter Ames was invented, which was only provided to the doctors [28] for diabetes testing. After that the diabetes detection method was not that much improved till 2004.

There are many hazards that diabetes can root like diabetic coma, kidney catastrophe, mental unevenness, etc. The good thing is, proper management/care cuts hazard complications pointedly for an eye ailment (76%), kidney infection (50%) and nerve syndrome (60%) [29]. Till 2014, 26 million Americans had diabetes and 1 out of 3 was not aware about that[30]. Moreover, 79 million [30] Americans are considered as "pre-diabetic" for not concerning about diabetes symptom and care. But till now for detecting diabetes the solution, lab or strip based methods are commercial. So, people are trying to find a unique way to make it easier.

The systems just discussed for sensing ethanol and diabetes has limitation on conversion of sensing and depends on the open system diagnosis, even, Henry's law does not precisely apply in the open system based breathing diagnosis. Moreover, blood-breath relation is extremely capricious[31] and the mediocre quality of the sample can cause false BAC. Though, in ethanol measurement there are several kinds of measurement type exists, such as wet-chemical (Breathalyzer), N-type semiconductor (Alcohol Interlock), Fuel Cell [32] and Infrared Intoxilyzer 8000, but still more easy, fast and accurate device to be made to detect alcohol. So, researchers are now focusing on material based sensitivity to develop new breathing sensors.

1.2 Literature review

For a few decades, many devices have been developed as POCT due to the revolution in the field of nanotechnology and nano-material. The sensor based POCT devices are more focused on two-dimensional 2D monolayer material along with the 0D quantum dots, 1Dnanotubes and 3D nanoballs/nanocones. In spite of the fact that graphene is the most quintessential two-dimensional materials, which is drawing in the consideration of the sensor analysts, however

there are some other sort of 2D metal oxides, hydroxides and chalcogenides, and metal-natural settings that can facilitate the manufacture of single layer material (table 1).

Table 1.1: Collection of 2D material.

Ternary 2D materials	Normal 2D material				Hybridized 2D materials
$WSe_{2(1-x)}Te_{2x}$	GaSe	InSe	$SnSe_2$	PtS_2	Bn
	WSe_2	In_2Se_3	h-Bn	$PtSe_2$	MoS_2
Ta_2NiS_5	WS_2	G	MoS_2	CdS	Pv
	$MOTe_2$	$MoSe_2$	ReS_2	CdSe	G
$ZnIn_2S_4$	BP	$TiSe_2$	$ReSe_2$	$PdSe_2$	Ruberene
		PbI_2	WTe_2		

Till now, huge scale business utilizations of 2D material with the exception of graphene are a fantasy because of their less accessibility. Aside from these difficulties, 2D graphene, Borophene, Silicene, Phosphorene, Hexagonal boron nitride and Molybdenum disulfide seemed helpful for sensor applications (fig. 1.1) [33].
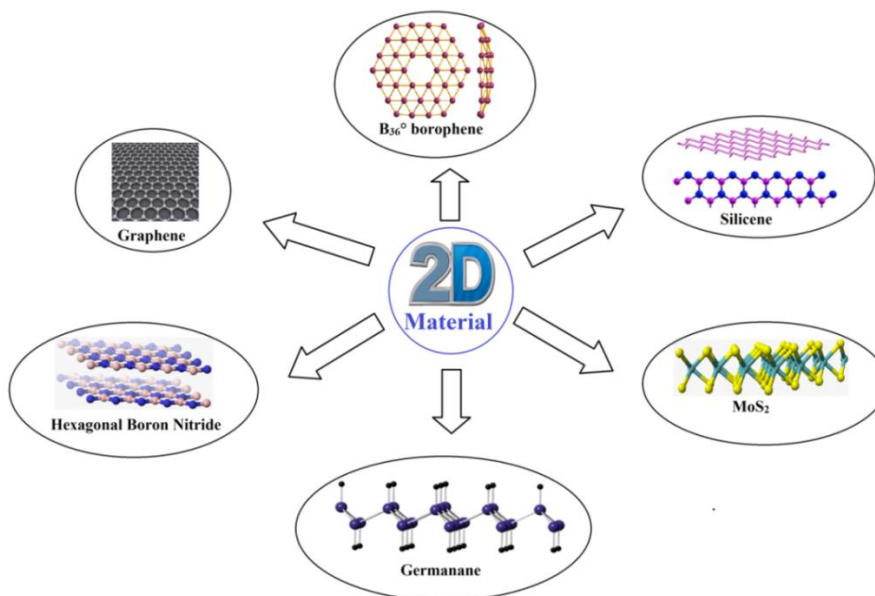
Figure 1.1. Most used 2D material in sensor application.

The breathing sensor is not that much stable field like the gas, electron, photonic or micro-fluidic sensing. Dr. Fan (2009) first stated about the trace of certain gas particles in the

breath due to the infrequent body issues [34]. He also tried to develop a sensor to detect certain molecules [35]. However, sensitivity of the sensor was not good for the distinct types of gases. Later, Song and his research group (2009) were developed an ethanol detector using SnO_2 nanofiber [36]. The detector was not compatible to detect diabetic or alcoholic breath. In 2013 Jungwoo Shin et al. first published a paper on Diabetes detection sensor devices Using SnO_2 nanoparticles [37]. The response time of the sensor was not that good. Usman latif et al. (2015) introduced graphene as a gas sensing material [38] to detect NO_2 or NO_3 gas. Till now the graphene is the most promising material in biomedical sensor based research.

There are many published works on graphene based chemiresistive sensors to detect NH_3 [39], NO_2 [39], pH [39], ssDNA [39], heavy metal like $Hg2^+$ [39]. It has been also used as Glucometers to detect glucose [40]. Recently, individuals are attempting to manipulate graphene structure for gas sensing [41] and SERS (Surface enhanced Raman spectroscopy) [42] application.

Another developing 2D Material past graphene is borophene, which is efficient in the detection of nucleobases A>G>C>T [43], toxic gases [44] and NO_2 [45-47]. It is also used in FET, CMOS, PMOS and NMOS transistor [48]. The Transition metal dichalcogenide (TMDC) monolayers are exceptionally compelling to distinguish DNA with 50pM limit of detection [49]. The figure below is showing the various applications of TMDs.
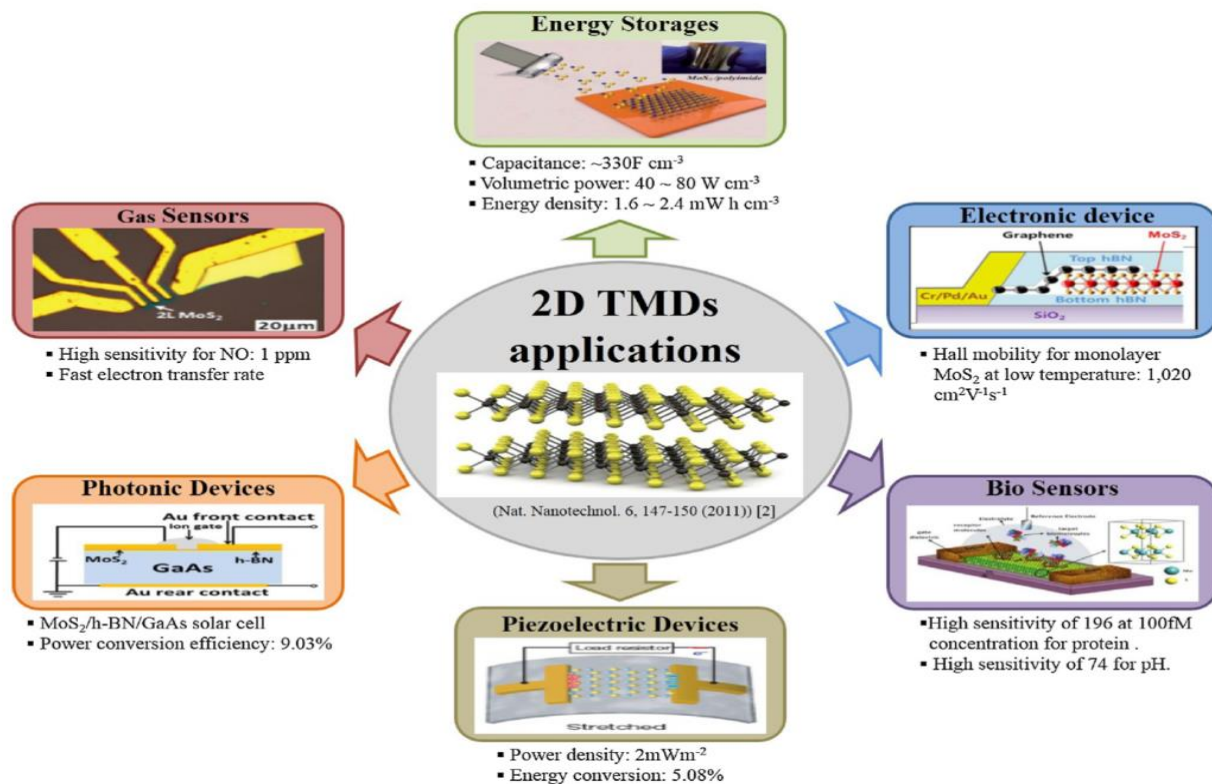
Figure 1.2.Progress and device applications of TMDs [1].

In the ancestry of TMD family, Molybdenum disulfide (MDS) can detect microcystin-LR [50, 51], hydrogen peroxide [52], glucose [52] and ammonia [53] with excellent semiconducting properties [54]. On the other hand, Hafnium Disulfide (HfS_2) is another TMDC which is potential to detect DNA sequencing. In contrast to the Hafnium based DNA detection, Hexagonal boron nitride (hBN) nanopores are extremely proficient in DNA sequence detection [55] along with UV light detection [56] and solid-state thermal neutron detection [57]. MXenes are also extremely reliable to identify nitrite [58]. Moreover, silicene is efficient to distinguish carbon, nitrogen and sulfur based gas molecules [59-62].

2D materials have efficient optical properties (Figure 1.3) [2], which can be utilized in solar cell application [63].
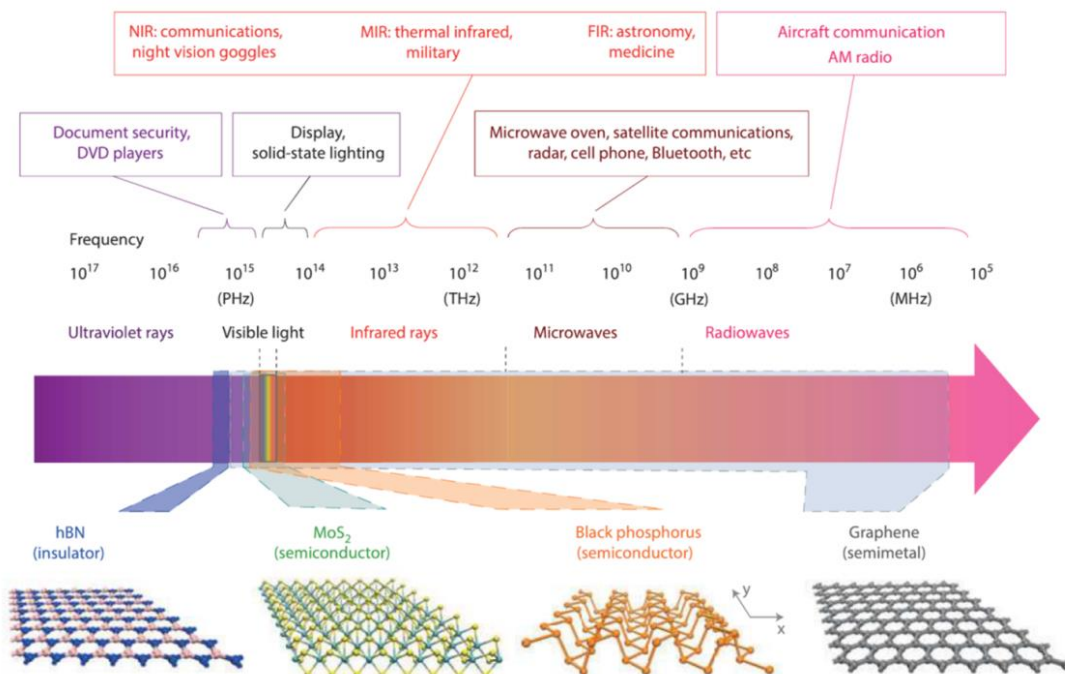
Figure 1.3. Optoelectronic properties of 2D materials [2].

Due to the excellent electrical and optical characteristics, it is very effective to use 2D material in sensor applications. Other materials like platinum, copper, silver and gold nanoparticles are also being used for sensing applications in the last couple of decades [64-74]. Those researches are the origin to develop breathing sensor technology. several material based work has been done to detect acetone and ethanol, such as graphene, tungsten trioxide, Crystalline ZnO nanoparticles (NPs), La doped ZnO nanofiber, indium nitride (InN), ZnO nanorods (NRs) doped with Co_3O_4 and Graphene/SiO_2 hybrid film [36, 75-86]. However, an individual may have acetone and ethanol molecule in breathing at the same time for biological issues, that can cause false detection [87-89]. Therefore, among all this works it is easy to understand that the graphene is very efficient to use in acetone and ethanol sensor. Even, graphene composites are also able to detect gases (table 1.2) [38, 90].

Table 1.2. Graphene and graphene composites in gas sensing.

Type of Graphene	Target Gas	Materials
Graphene	NO_2	Epitaxial-G, G-ozone treated, G-exfoliated, G-nanomesh
	NH3	G-nanomesh, rGO, G-microfiber
	CO_2	rGO, Graphene sheets
	H_2	rGO
Graphene polymer hybrids	NH_3	G-PEDOT-PSS, PMMA-rGO, PPy-rGO, PPy-rGO, rGO-PANI, rGO, rGO-PPy
	NO_2	PEDOT-rGO, rGO nanofiber, rGO-PPy
	$N(CH_3)_3$	G-Nylon 6
	DMMP	rGO-PPD
graphene metal/metal oxide hybrids	H_2	PMMA-Pd NP-SLG, Pd-GNR, Pd-WO_3-rGO, G-Pt/Pd, Pt-NG/Pt_3Fe-NG, G-ZnO, rGO-SnO_2 QDs, rGO-Pt
	NH3	rGO-Pt, G-mica, SnO_2-G, TiO_2-PPy-G, ZnO-GO
	NO/NOx	rGO-Pt, GO-Au NPs, ZnO-GO, $Co(OH)_2$-rGO, CuO-G, rGO-Cu_2O, In_2O_3-G, Co_3O_4-rGO, rGO-CNT-SnO_2, SnO_2-rGO, GO-Cs
	C_2H_2	Ag-ZnO-rGO, SnO_2-rGO,
	CH_2O	ZnO-G
	$(CH_3)_2CO$	G-$ZnFe_2O_4$
	C_2H_5OH	G-ZnO
	CO	ZnO-GO, GO-Au NPs
	CH_3OH	Co_3O_4-rGO
	H_2S	Fe_2O_3-G, G-SnO_2, MoO_3-rGO

The production of stable graphene solution is still a challenge to win. Different sophisticated techniques for ultrathin graphene layer fabrication, such as spin coating, drop casting or inkjet printing cannot be pragmatic for synthesizing ultrathin graphene layers. Among them, only spin coating method is good to control the film thickness. However, the spray coating and drop casting method are also easy to proceed, but they often yield rough surface due to the unwanted particle size in the solution. There are lots of methods that researchers were adopted previously to make suspension free graphene solution. DMF, NMP, THF and ethylene glycol can form firm graphene oxide dispersion that lasts for long time [91]. However, the graphene exfoliation method was achieved a milestone in 2010, when the ultracentrifugation-free solution was made by adding stabilizing polymer [92]. It is very easy to fabricate graphene layer by following this ultracentrifugation-free procedure.

Natnael et al. proved that liquid phase dispersion can produce a better graphene solution [93]. In contrast to that, Zhang and coleman (2010) presented Acidic dispersion method, which can be very useful to trim down the flake area or graphene with 75% solubility [94]. They also proved that the ethanol is a very good solvent for dispersing graphene. Later, Arlene O'neill (2011) stated that the low boiling point solvent based graphene dispersion can reduce the suspension problem [95]. After that, solvent exchange exfoliation with nano-platelates mixing was introduced by Jaiseng et al. in 2014 [96]. This method is efficient to increase the stability of the graphene solution by decreasing suspension problem.

In summary, the diabetes and alcohol sensor technology have been improved by using various material, method and technique in the last couple of years. It is already established that the graphene is the most appropriate gas sensing material. Even more surprisingly, it is already used in wellness sensor [97], strain sensor [98-100] and biosensor [101]. Unfortunately, the

sensors are often affected by the ambient environment. Thus, molecular imprinting technique is being adopted in this work to detect specific molecules.

1.3   Motivation and objectives

There is a need to design highly sensitive and selective breathing sensors.

The goal of this work is to develop molecular imprinted filter based breathing sensors to detect diabetes and alcohol biomarker. To achieve this goal, the following tasks were performed.

1) Processed spray coat-able Graphene nanoplatelets based stable solution with super binding capability with plastic.

2) Synthesized molecular imprinted (MI) filter layer by combining poly-Ethelene glycol and SnO_2 nanofiber with acetone or ethanol.

3) Optimized the thickness of graphene and MI layer.

4) Modified the selectivity of the diabetes and alcohol sensor by using MI layer.

5) Characterized the quality and performance such as limit of detection (LOD), repeatability and stability of the sensors with optimized exposure time.

1.4   Organization of the thesis

Chapter 1 describes the necessity of designing highly sensitive and selective breathing sensor to detect diabetes and alcohol. A brief history of the diabetes and alcohol sensor based research approaches along with challenges of the molecule based detection is stated. Finally, the motivation and objectives of this work are conscripted.

Chapter 2 informs about the theory and models of adsorption process. A detailed working principle of molecular imprinted filter along with the molecular activity is interpreted. Several characterization processes through the whole research work are also enlisted with important sensors parameters.

Chapter 3 delivers about the development processes of the diabetes and alcohol sensor. Moreover, it clarifies all the subtle issues of fabrication process.

Chapter 4 discusses about the results, analysis and performance of the sensors.

Chapter 5 concludes the work pointing out future plans.

Chapter 2: Theory

2.1   Adsorption

Most of the commercial gas sensors work on three types of principle - absorption, adsorption and desorption (fig. 2.1). The absorption mechanism is linked with the dissolution of gas, liquid, or solid molecules to a surface. In adsorption, no particle dissolution happens, but the adsorption evolution forms a layer (single or multiple) of the adsorbate on the surface of the adsorbent or adsorbent site. The other procedure named desorption can happen if the equilibrium condition for absorption or adsorption changes.
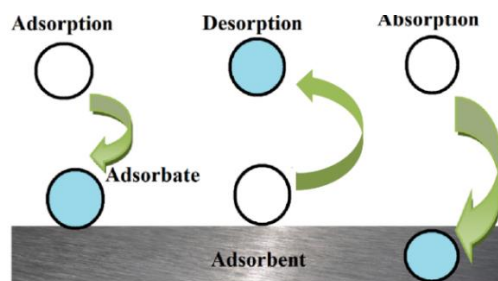
Figure 2.1. Adsorption, absorption and desorption processes.

The fig. 2.1 shows the adsorption process along with the absorption and desorption. The surface tension and surface energy of the adsorbent layer depend on the bonding type and position of the atoms. In the bulk structure, atoms are so compact that limits the adsorption process. Even, according to the Lennard-Jones potential the adsorption increases with the increase of bond energy (ε) (figure 2.2).
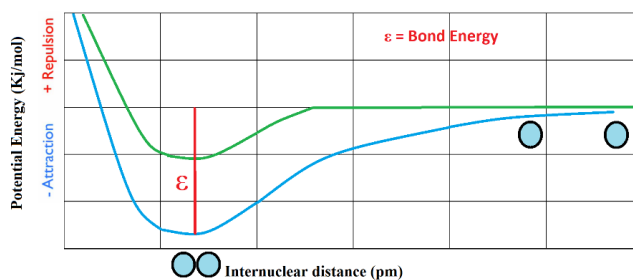
Figure 2.2. Lennard-jones potential curve for surface (blue) and bulk (green) atoms [102].

The adsorption method is classified in two categories - weak van der Waals forces driven physisorption and covalent bond driven chemisorption. Except some rare case, chemisorption based sensors are unfriendly of adsorption and irreversibility; limits the reusable feature of sensor [103]. The word "adsorption" was carried out by German physicist Heinrich Kayser in late 1881 [104]. Graphene has two kinds of bond – sigma (σ) and pi (π) bond and both of them are able to interact to detect acetone and alcohol [105]. The figure below is showing the interaction of acetone and ethanol with the graphene.
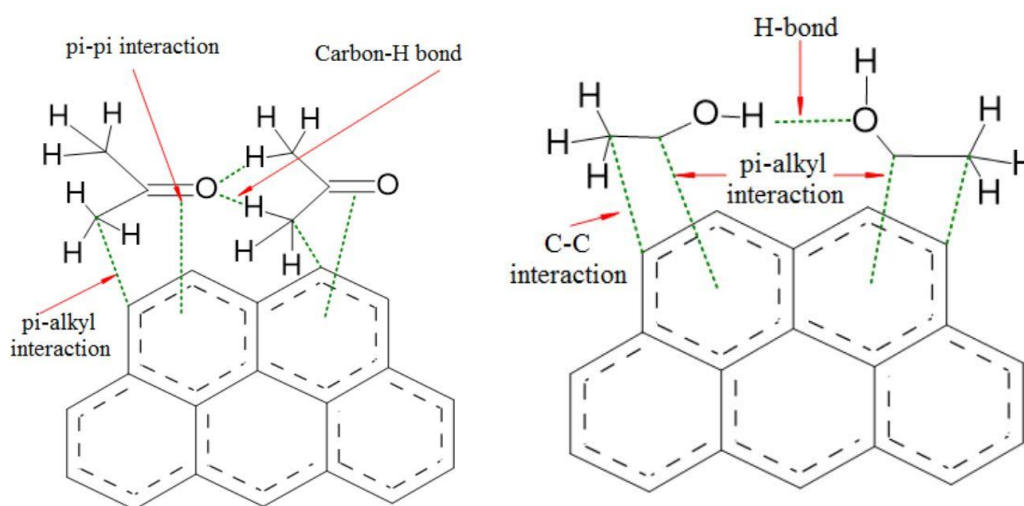
Figure 2.3. Distinct types of interaction of acetone and ethanol interaction.

In acetone sensor, there are two kinds of interaction happen - π-π and π-alkyl interaction. Later, enough adsorbate (acetone) is adsorbed, and then a weak C-H bond starts to establish, called intermolecular interaction. In case of ethanol adsorption, C-C and π-alkyl interaction dominates the adsorption process. But, in the presence of the excess ethanol molecule a H-bond starts to develop between the ethanol molecules as intermolecular interaction. All this interaction will reduce electron flow through the graphene layer with increasing the sheet resistance. Here to say that, the adsorption dynamics is a continuous process which is often a bidirectional/reversible or equilibrium reaction.

$$\text{Adsorbate} + \text{Adsorbent} \rightleftarrows \text{Adsorption product}, \ldots. (1)$$
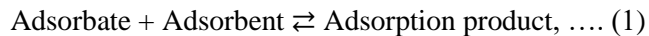
The equilibrium relationship is usually described by isotherms and it shows the relation between the adsorbate on the adsorbent as a function of concentration. The nature of the adsorption can be expressed as Langmuir Isotherm (form I), $q = \frac{q_m K_L C}{1 + K_L C}$ …. (2) [106], Where q defines adsorption capacity of adsorbent, q_m is the maximum adsorption capacity, K_L is known as Langmuir equilibrium constant and C is the equilibrium concentration. In equation 2, $q \propto c$ and they are linearly correlated. The figure 2.4 shows the characteristics or the Langmuir equilibrium.
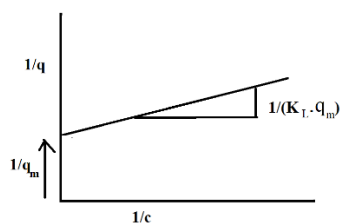
Figure 2.4. Langmuir Characteristic.

Langmuir model is verified only when the surface will be homogenous with identical single layer adsorption site. If the adsorbate molecule interaction increases, the Langmuir isotherm becomes invalid [107]. Then adsorption nature changes from Langmuir to BET isotherm (form II), which is multi-layer adsorption (figure 2.5).
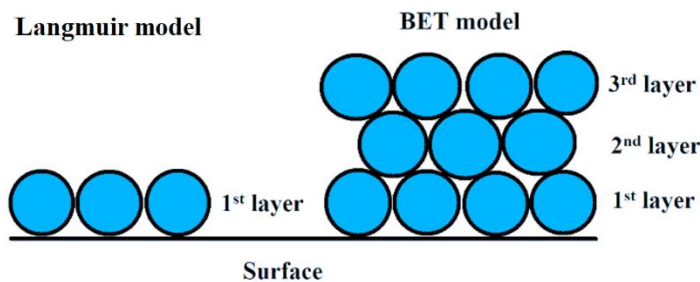
Figure 2.5. Layer based Langmuir and BET adsorption model.

The BET model is the further derivation of the Langmuir equation. It defines the saturation concentration of the adsorbate that will be adsorbed and expressed as, $q = \dfrac{q_m K_L C_e}{(C_s - C_e)[1 + (K_L - 1)\frac{C_e}{C_s}]}$ …. (3), Where, C_s defines the saturation concentration and C_e is the equilibrium concentration. Further derivation of equation 3 leads to $q \propto \dfrac{C_s}{(C_s - C_e)}$. The figure below shows the characteristics of BET model.
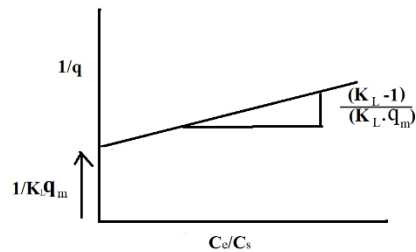
Figure 2.6. Characteristic of BET model

There is another isotherm called Freundlich model and expressed by, $q = K_F \cdot C^{1/n}$ …. (4), where, K_F and n (0.1~ 0.5) are Freundlich equilibrium constants. The value of 1/n defines the amount of resistance of the sensor (Fig. 2.7).
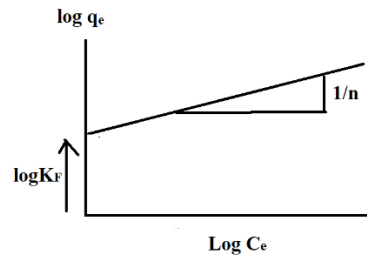
Figure 2.7. Characteristic of Freundlich equilibrium.

The typical real-time characteristics of Langmuir, BET and Freundlich adsorption model are shown below in equilibrium condition,
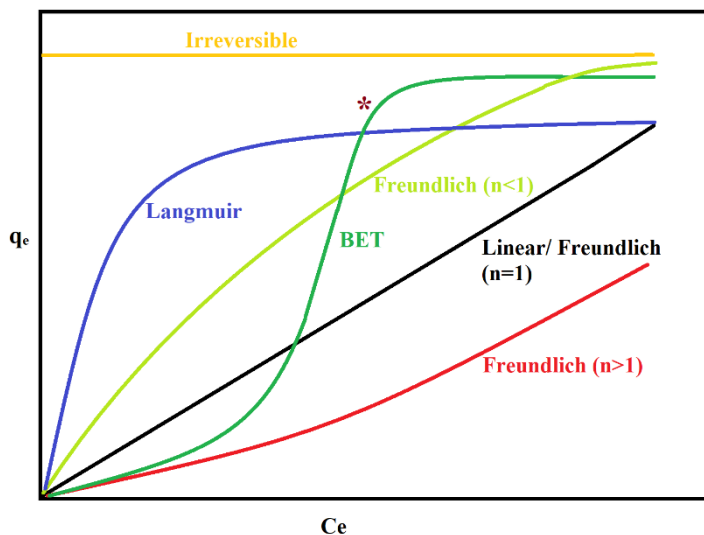
Figure 2.8. Characteristic curves of adsorption models (*saturation concentration of the adsorbate).

The Langmuir, BET and Freundlich characteristics are often observed in the water or gas adsorption. However, The uncommon BET (figure 2.8 - green) characteristic is usually exhibited in gas adsorption on mesoporous or rough solids [108]. Langmuir and Freundlich (n≤1) are very favorable while the Freundlich (n>1) is extremely unfavorable. According to the all characteristic curves, concentration of the adsorbates (C_e) and amount of adsorption (q_e) are proportional, that leads to the higher amount of C-C interaction in Ethanol and π-π interaction in acetone. Consequently, the resistance of the graphene layer will be increased and current flow thorough the layer will be decreased.

2.2 Molecular imprinting

The molecular imprinting (MI) technique is excellent to detect specific molecules. It is a polymer science based technology. Several macromolecules such as viruses [109], bacteria's [110], proteins [111], antibodies [112], pathogens, enzymes [113], nucleic acids [114] and tumor cells [115] are tough to detect, but the imprinting technology has given the opportunity to detect those with low cost, high specificity and stability.

The molecular imprinting was first invented by the Wulff and Sarhan in 1972 [116]. It is just like finding the missing parts of a puzzle (fig 2.9a). Chemically, it is a functionalization process between target molecule and functional monomer (cross-linker). The functionalization process creates a cavity (fig 2.9b) in the polymer template. These cavities are the host to detect the target molecules.
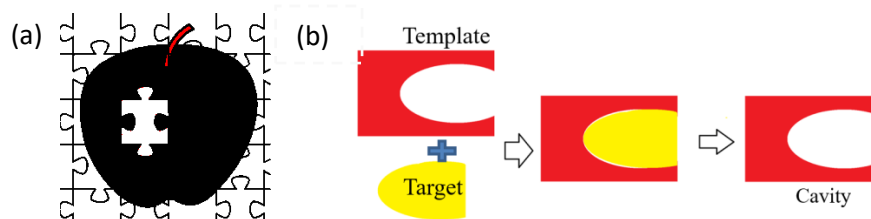
Figure 2.9. Molecular imprinting logic (a) and theory (b).

There are three types of molecular imprinting technique [117]. The surface modified imprinting technique is used in agriculture to detect atrazine (herbicide) in the aqueous solution. The atrazine extraction from the template solution creates the imprinted sites, that later detect atrazine [118]. The whole atrazine detection by surface modified imprinting technique is shown below.
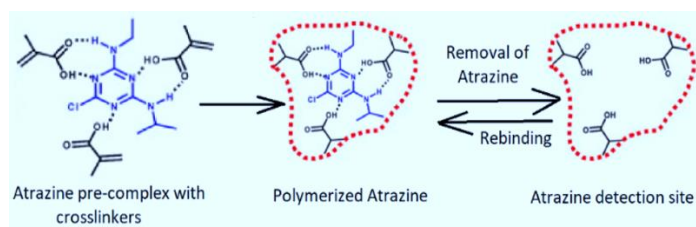
Figure 2.10. Atrazine detection sensor[3].

The figure 2.11 is the clear representation of the microcontact imprinting on Sepiapterin Reductase (SPR) chip. A separate glass slide containing pre-complex (template) film is usually attached with another glass slide that contains monomer solution [118]. After removing the template, imprinted site appears on the monomer film , that works to detect specific protein.
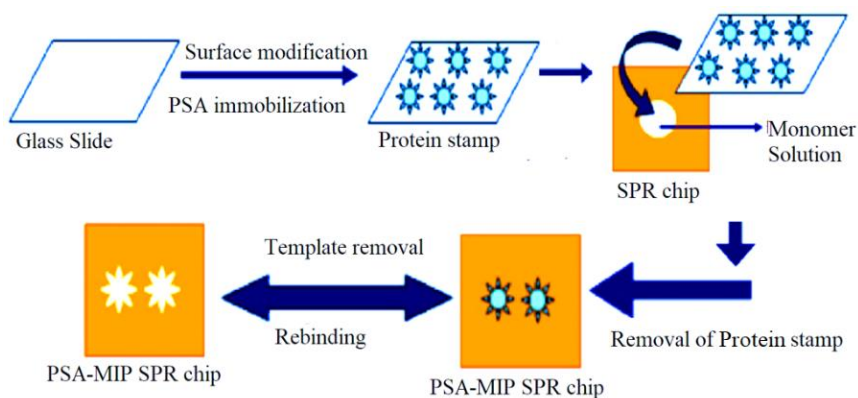
Figure 2.11. Microcontact imprinting [4].

The Fig. 2.12 shows the epitome imprinting techniques of protein, where the whole protein is not needed to be imprinted on the film. Only a portion of the protein is necessary to imprint for successful detection [118]. That kind of imprinting technique is used in the sensor to detect HIV.

Figure 2.12. Epitome imprinting of protein [5].

In this work, the surface imprinting technique is used to detect acetone and ethanol molecule separately. The acetone or ethanol imprinted layer is fabricated over graphene layer separately to work as a filter (fig. 2.13). However, nearly same kinetic diameter of acetone and ethanol molecules (table 2.1) is a challenging issue to overcome for successful imprinting.
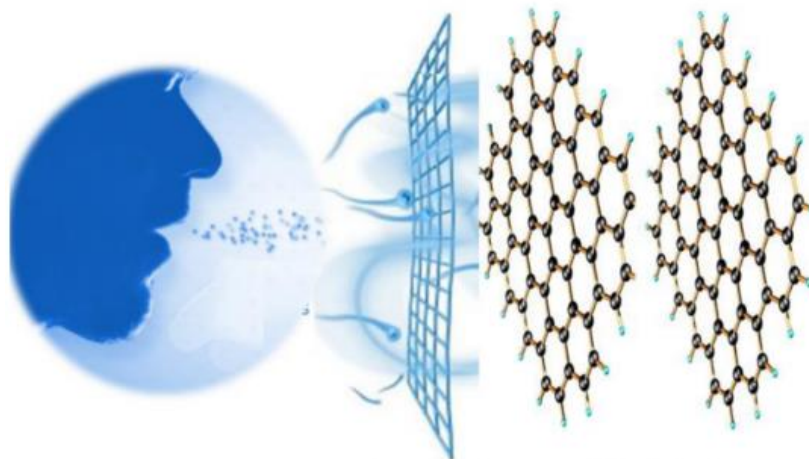
Figure 2.13. Molecular imprinted filter theory.

Table 2.1. Kinetic Dimeter chart of different molecules

Molecule name	Kinetic diameter (nm)
IPA	1.605
Ethanol	0.45
Acetone	0.48
Water	0.275

The novel approach in this work is to use the acetone or ethanol imprinted polymer layer as a filter. Moreover, acetone is a porogenic solvent [119] and it will weakly interact with PEG (reversibly) in solution. Furthermore, it will also leave pores of a specific size on polymer matrix, that will enhance the acetone molecule penetration through the filtering layer. The figure below shows the interactions between acetone and PEG.
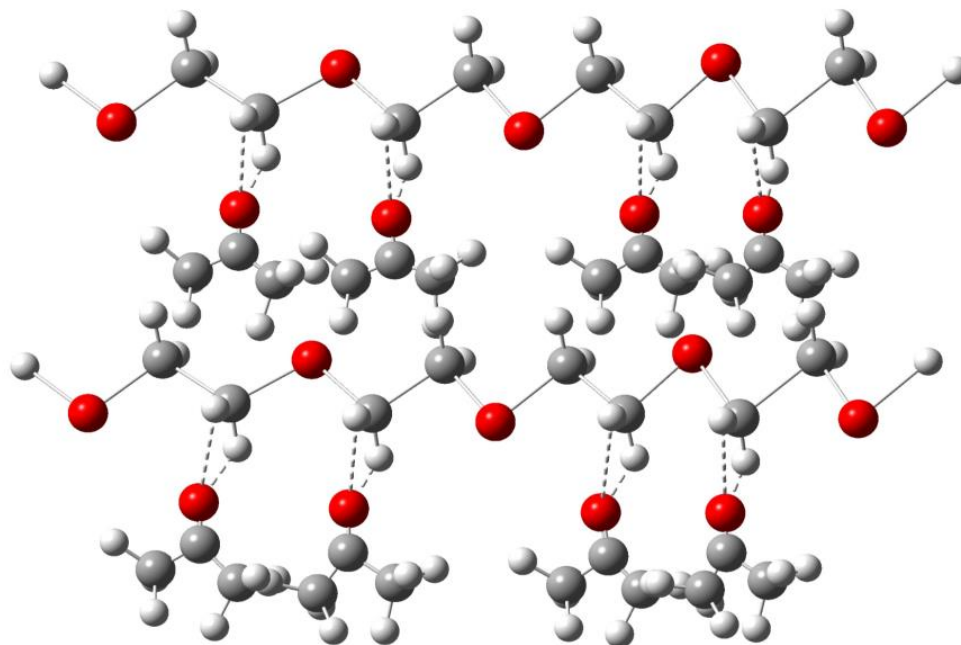
Figure 2.14. C-H…O interaction between acetone and PEG.

In case of ethanol, the hydroxyl (-OH) group yields hydrogen bond based interaction with other molecules in liquid phase [120]. Therefore, in the PEG and ethanol mixture, an H-bond based interaction happens (figure 2.15). Later, the annealing process removes the ethanol and creates a ethanol imprinted layer on PEG template.
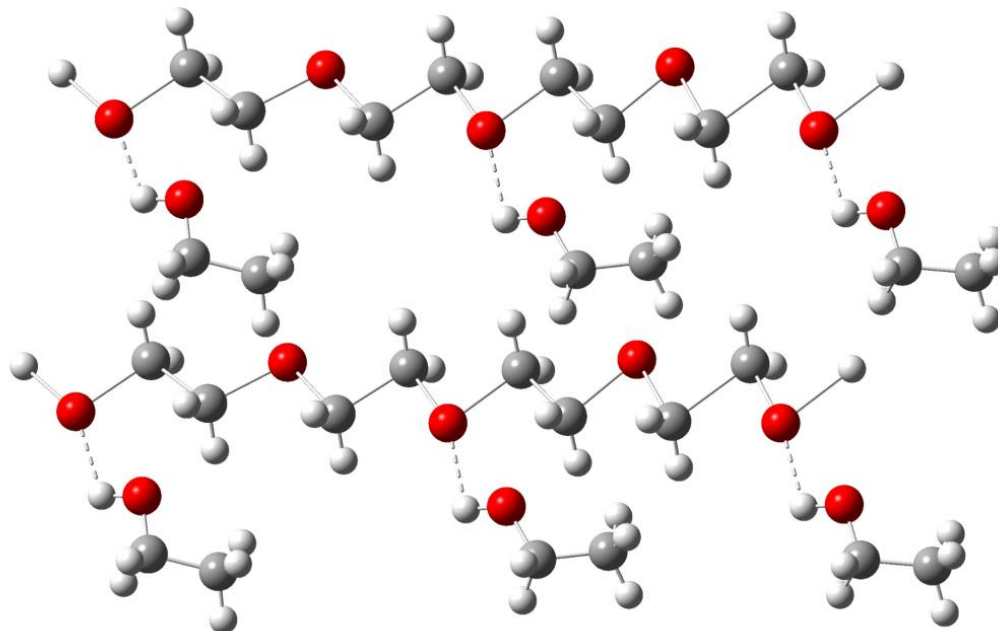
Figure 2.15. H-bond between ethanol and PEG

2.3   Device Structure and circuit connection

The sensor has two-layer fabricated on a plastic (polyethylene) substrate. The first layer is made of graphene and the molecular imprinted second layer is fabricated over graphene layer. The device structure is shown below.
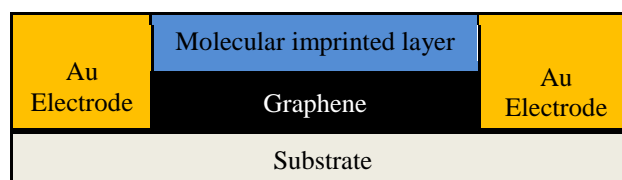
Figure 2.16. Sensor device structure.

The supportive circuit connection for sensing is also very simple (fig. 2.17). It has a voltage source incorporated with the sensor and LED. The voltage source recurrently supplies voltages to the sensor. When the sensor is exposed by the acetone or ethanol, a resistance change will switch the LED in on/off position (depends on circuit design).
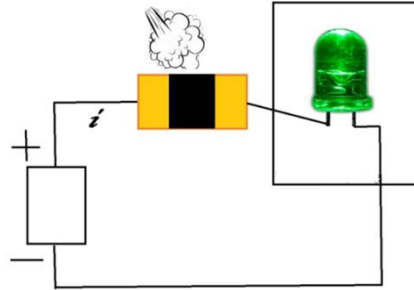
Figure 2.17. Electrical circuit diagram and connection of the sensor devices.

2.4   Sensing parameters

The resistance of the graphene layer is the main sensing parameter that gives the level of sensing. The unexposed resistance of the graphene sheets is called resistance of the sensor in air denoted by R_{air} which changes to R_{gas} when the sensor is exposed to the acetone or ethanol. The difference between the R_{air} and R_{gas} is the parameter to sense. Resistance sensitivity is denoted by $R_{sensitivity}$.

$$R_{sensitivity} = (R_{air} - R_{gas})/\text{Concentration difference} \ldots (5)$$

As the resistance of the graphene sheet is changing due to the adsorption of the acetone and ethanol, that enables the change in current flow thorough the graphene. The current amount in the unexposed sensor is denoted by I_{air} and I_{gas} is the amount of current in the exposed graphene sheets.

$$\text{Current sensitivity, } I_{sensitivity} = \frac{I_{air} - I_{gas}}{I_{air}} \ldots (6)$$

Though in this work the current level detection is not the main theme as sensing parameter, but it plays a key role in the circuit base analysis of the sensor. Gas response is another important parameter, which means the amount of the change in resistance per ppm in the unexposed and exposed film. It also calculated using the change of the resistance. The more the gas response happens, the better the sensitivity of the sensor is expected.

$$\text{Gas response} = \frac{R_{air}}{R_{gas}} \ldots (7)$$

Percentage sensitivity is another parameter, which is similar to the gas response. only the unit is in percentage scale.

$$\text{Percentage sensitivity} = \frac{R_{air}}{R_{gas}} \times 100 \ .... \ (8)$$

Additionally, the limit of detection (LOD) is the lowest concentration of the target that can be detected by a sensor. it is a standard deviation based numerical analysis. It is not always possible to measure the sensitivity of the sensor at the LOD level. Sometimes, it is only a calculated value. To estimate the LOD of acetone and ethanol sensor the equation below can be used –

$$\text{LOD} = 3.3 \times \left(\frac{SD}{s}\right) \ .... \ (9)$$

"SD" defines the standard deviation of the signal (resistance of the graphene layer without exposure in that work) and follows - $\text{SD} = \sqrt{\frac{\sum_{i=1}^{n}(x_i - \bar{x})^2}{n-1}}$ ... (10). "S" denotes the slope of the sensitivity curve and follows the equation, $\text{S} = \frac{\Delta y}{\Delta x}$ ... (11). In SD calculation, n = the number of the data points, $\bar{x}$ = the mean of x_i and x_i = each of the values of the resistance per exposure. In addition, Δy = change in y axis (resistance) and Δx = change in x axis (exposure) in between 2 data points of the curve.

The another most important parameter of sensor is repeatability. It defines the number of successive occurrence of same sensitivity in the same location under identical conditions. In the linear measurement systems, the repeatability can be a comparison between the sensitivity curves of the sensors. In this work, maximum likelihood (ML) vs. weighted Least Squares (WLS) approaches were used to evaluate the repeatability. They are very efficient tools [121] to infer the convergence or deviation between curves. The sensitivity deviation analysis by ML and WLS follows equation 12 and 13.

$$\text{ML method:} \ \frac{1}{n}\sum_{i=1}^{n}\left|1 - \frac{observed\ value_i}{expected\ value_i}\right| \ .... \ (12)$$

$$\text{WLS method: } \frac{1}{n}\sum_{i=1}^{n}\left|1 - \frac{Expected\ value_{i}}{observed\ value_{i}}\right| \dots (13)$$

The stability of the sensor deals with the degree to which sensor features persist continuously over time. The equation 14 was used to find out the stability of the sensor over a period.

$$\text{Stability} = \frac{Observed\ resistance\ value}{Expected\ resistance\ value} \times 100 \dots (14)$$

However, stability can be affected by mechanism aging, reduction in material sensitivity, alteration in the signal to noise ratio. Moreover, Physical or chemical fluctuations can cause calibration drift in the sensor. In this novel work, stability of the sensors was determined on the base of sensitivity and gas response of the sensors over a certain period.

2.5 Working principle of characterization techniques

2.5.1 Scanning Electron Microscope (SEM)

An electron gun of the scanning electron microscope directs electrons to the sample. A dedicated electromagnetic lens and detector analyzes the outgoing electrons or x-rays (fig. 2.18) from the sample. SEM helps to gather information about the sample surface. In the acetone or ethanol sensor the graphene layer surface is a very important factor. If the defect is too high, then the sensitivity to the ambient molecules will be increased and selectivity will be poor. Therefore, SEM is used to characterize the defects and homogeneity of the graphene and molecular imprinted layer.
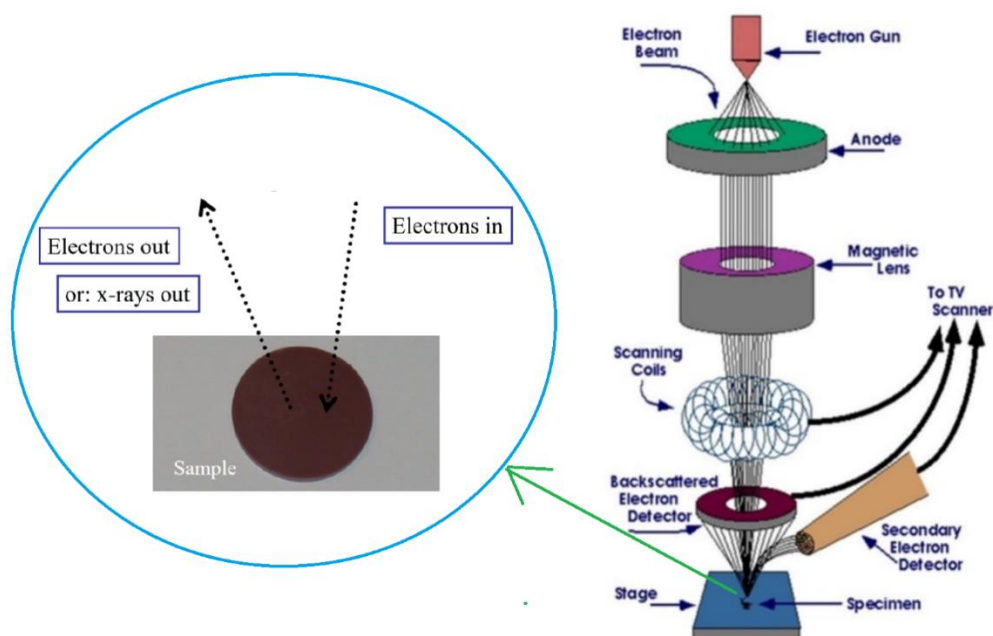
Figure 2.18. SEM working principle [122].

Several materials can be investigated by SEM, such as metals, glass, ceramics, semiconductors, plastics, polymers, powders, dust and composite materials. From the sample three things comes out, such as backscattered electrons that provides compositional contrast with brightness, secondary electrons (SE) that gives topographic information and fluorescent X-Rays, which can give material composition.

2.5.2   Raman Spectroscopy

Raman is a spectroscopic technique that aids to observe vibrational, rotational and other low-frequency signal generating from the scattering of a sample surface by introducing a laser excitation (fig. 2.19b). Raman spectroscopy is frequently used in chemical analysis. It can acknowledge specific fingerprint of a material. Particularly, this method is effective for particles with altering polarization. The transformation in the polarization transpires when the particles are in an electrical field.
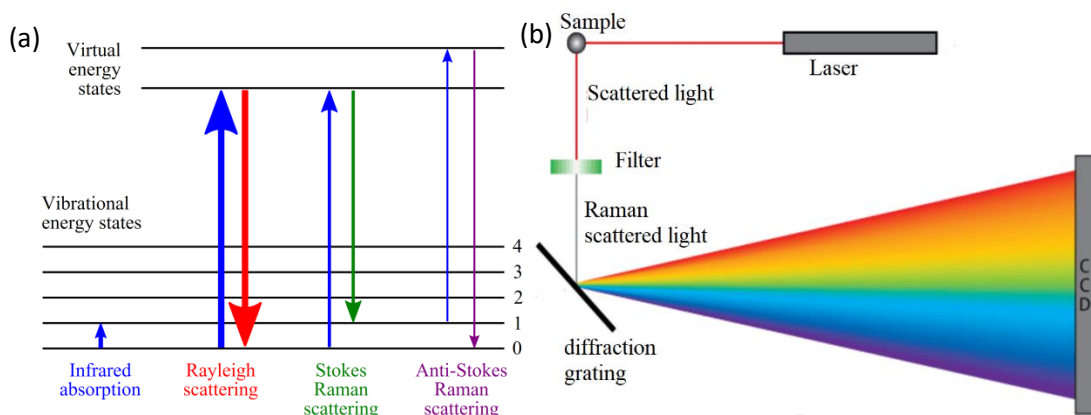
Figure 2.19. a) State diagram of different scattering [6] and b) Raman instrumentation diagram [7].

There are several states or energy level that is responsible for Raman signal (fig. 2.19a). If the photon and molecular interactions (vibration/rotation) frequency matches the light is captivated by that molecule. There are three different radiation frequencies usually observed. Rayleigh scattering happens when the incident and radiated light is equal. Raman can't detect that, as no absorption happens due to the elastic transition between energy levels. Stokes Raman scattering takes place, when radiated and incident light is not equal and Raman active (inelastic) anti-stoke Raman scattering enables when the radiated light is equal to the combined incident and absorbed light.

Raman is not only for detecting the molecules, but also an effective tool to give information about the film quality. There are four things that can be analyzed by Raman, such as band width, band position, band shift and band intensity. The peak position for specific material is always fixed in Raman spectrum. The bandwidth refers to the quality of the film and structural disorder in the material. Besides, the band intensity provides information about concentration and band shift refers to the mechanical or thermal effects on the lattice [123, 124].

In case of graphene, the Raman spectrum gives 3 peaks G, D and 2D peaks/band. The G band refers to the graphene or monolayer graphene. The D band is appeared due to the disordered portion of graphene in the film. Furthermore, a highly disordered band 2D appears, which is an

overtone of the G and D band. The Position of those peaks depend on the number of layer. If the layer of graphene increases from single to multiple layers the peak positions changes accordingly. For single layer graphene the G, D and 2D position are fixed and appear in 1400 – 1600 cm^{-1}, 800 – 1400 Cm^{-1} and 2500-2800 cm^{-1} respectively (fig. 2.20) [8]. However, defects in the film can affect the peak position and intensity [125].
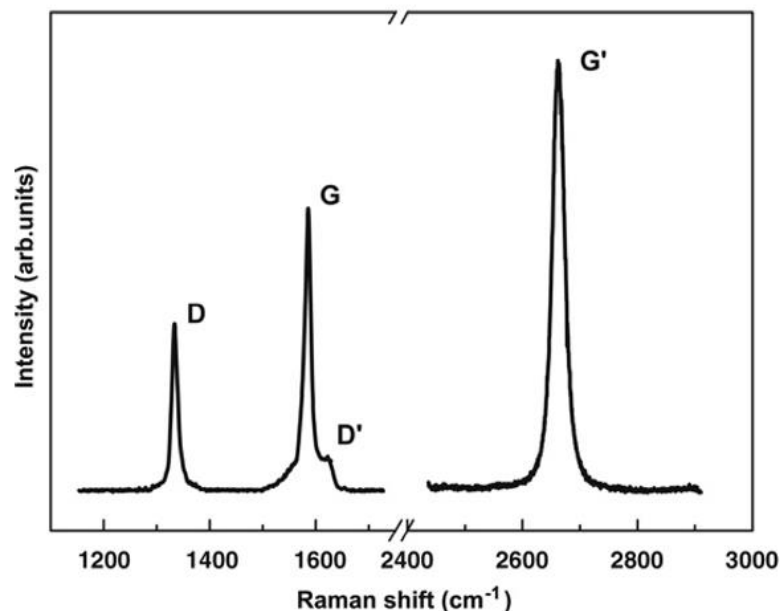
Figure 2.20. Raman spectrum of graphene [8].

There are two types of diffraction grating (300 and 1800), four kinds of objective lens (10x, 20X lwd, 50x and 100x), four kinds of lasers (325nm, 532/530nm (Green), 633nm, and 785nm (Red)), and six types of filters (D 0.3, 0.6, 1, 2, 3 and 4) in Raman spectroscopy to improve the spectral analysis.

2.5.3 Fourier transform infrared spectroscopy (FTIR)

Infrared spectroscopy (IR spectroscopy) is another spectroscopic method that pacts in the infrared section of the electromagnetic spectrum (4000 and 400 cm^{-1}). IR spectra results from molecular vibrations and change in the dipole moment in an organic molecule. It gives

information about functional groups present in the sample. Like Raman, every molecular species and structure produces a different infrared spectrum but specific for a particular material.

A communal FTIR spectrometer entails of a source, interferometer, sample compartment, detector, amplifier, A/D convertor and a computer (figure 2.21). The source stimulates radiation that goes through the interferometer, sample and then reaches to the detector. The signal is relocated on a computer screen to execute the Fourier transform.
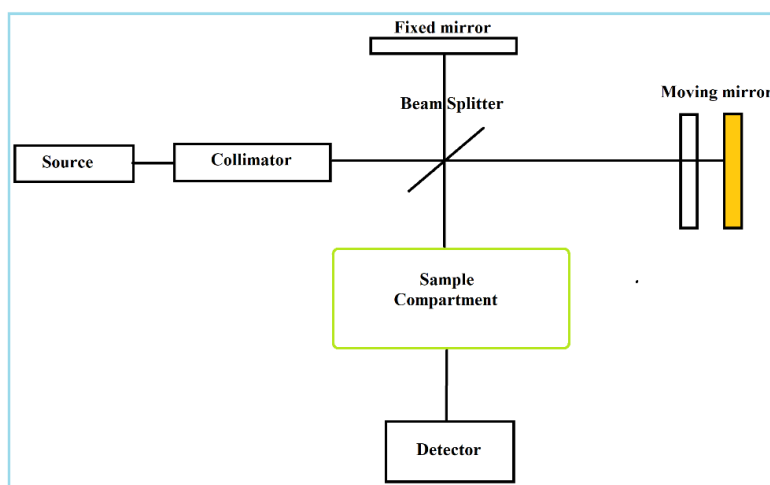
Figure 2.21. Block diagram of a FTIR instrument [9].

2.5.4 Attenuated total reflectance (ATR-IR)

Attenuated total reflectance -IR is another accessory that passes an IR beam as evanescent wave through the sample to take the spectroscopic data by using a diamond tip. The ATR-IR can examine the surface property without special sample preparation. The functional group of acetone (C=O) and ethanol (O-H) can be identified by ATR-IR spectra while exposing [126, 127]. Moreover, the figure 2.22a below is showing the typical ATR spectroscopy configuration and 2.22b is about infrared absorption frequencies of different functional classes.

Functional group	Absorption location (Cm^{-1})
Alkane (C-H)	2850 - 2975
Alcohol (O-H)	3400 - 3700
Alkene (C=C)	1640-1680
(C=C-H)	3020 - 3100
Alkyne (C≡C)	2100 – 2250
(C≡C-H)	3300
Nitrile (C≡N)	2200 - 2250
Aromatics	1650 - 2000
Amines (N-H)	3300 - 3350
Carbonyls (C=O)	3000
Aldehyde (CHO)	1720 - 1740
Ketone (RCOR)	1715
Ester (RCOOR)	1735 - 1750
Acid (RCOOH)	1700 - 1725
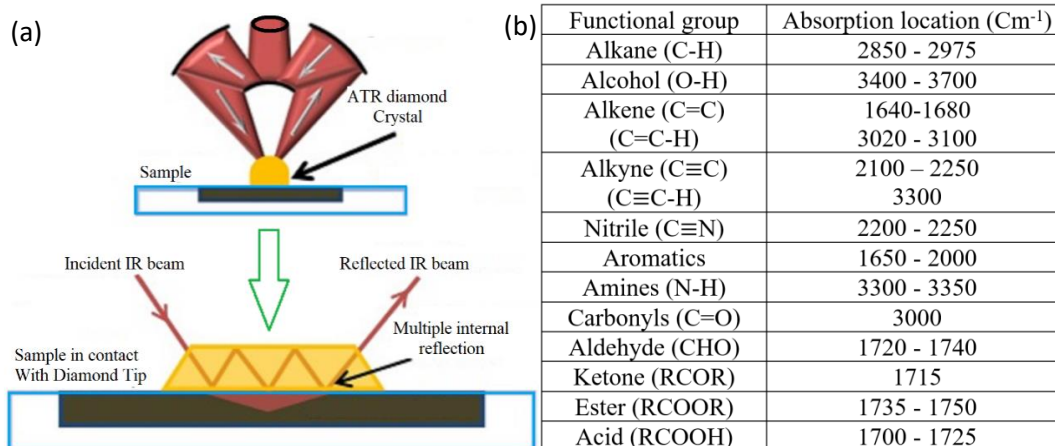
Figure. 2.22. a) ATR-IR working principle [10] and b) position of functional groups in IR spectrum [11].

2.5.5 Dektak profilometer

It is a Stylus or probe method to measure the surface roughness and thickness. A tip usually takes the surface data in one dimensional direction by contact or non-contact method. In optical method, a source passes a light on the stylus mirror, while a photographic film detects the movement of the stylus. However, in the Daktak profilometer the stylus uses a tip force or stress based analysis to collect the surface data (figure 2.23). It is the easiest way to collect surface profile along with the information of roughness of the film.
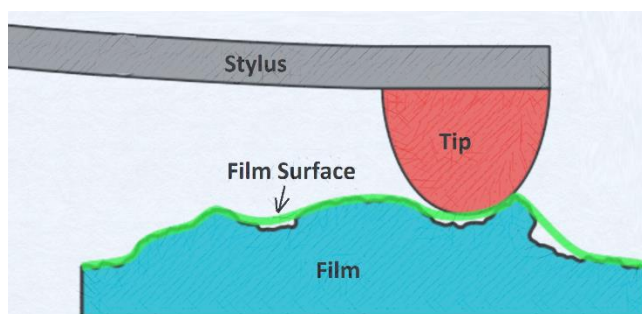
Figure 2.23. Profilometer working mechanism.

2.5.6 Semiconductor parameter analyzer

It is very useful to extract the IV analysis of the sensor, Diodes, BJTs and MOSFETs from 0 – 1 volt range. The I-V characteristics of the sensors were analyzed by the Agilent 4155C semiconductor parameter analyzer. However, a high-power DC supply works as a source and it has four terminals - two for the source and measurement and another two for Kelvin connection.

Power is concurrently sourced or sink to the terminal pair at the same time to measure the current or voltage across those terminals. An integrated current and voltmeter are also added for taking the current and voltage data [128]. The figure below shows the I-V measurement unit.
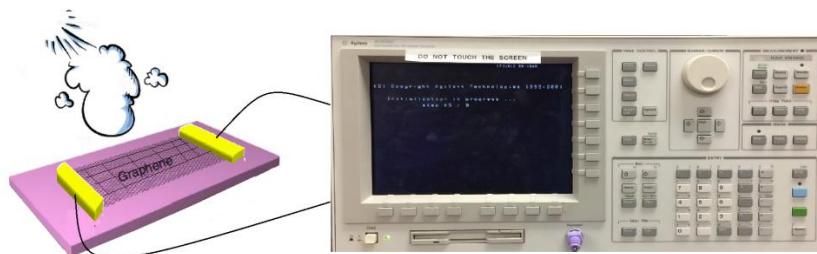
Figure 2.24. Complete I-V measurement Unit.

2.5.7   Rotameter

It is a device that can measure the air flow in cc/min created by an air blower. It has one inlet and one outlet in a closed chamber, where a small moving ball with specific weight gives the indication of about how much gas or air is flowing inside. The maximum permissible operating temperature inside the Rotameter is 37.9^0C. The circular knob in front of the Rotameter can control the flow of the air inside the chamber. The Rotameter or Flowmeter setup is shown in the figure 2.25. This setup is being used in measuring the selectivity of the sensors to the acetone, ethanol, dry air (relative humidity is 5.52% and dew point $– 1^0$ F) and wet air (relative humidity is 90% and dew point 69^0 F).
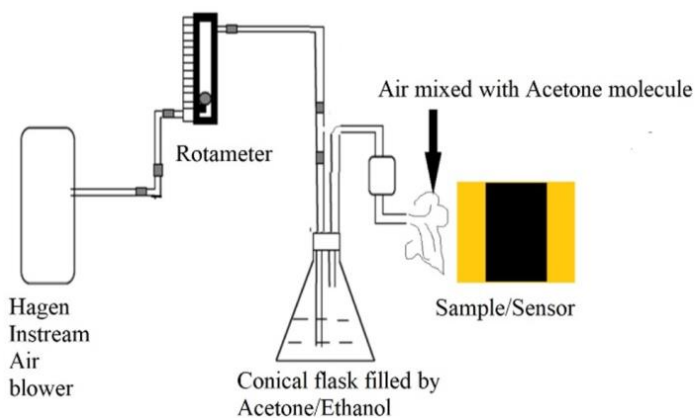
Figure 2.25. Rotameter setup for sensitivity measurement.

2.5.8   Part per million (ppm) measurement unit

The diabetic and alcoholic patients has ppm amount of acetone and ethanol in breathing. Therefore, the exposure amount to the sensor and the sensitivity of the sensor should be extracted by exposing acetone or ethanol of ppm concentration. A very conventional way has been developed by using a big conical flask filled with predefined (1 µl of acetone/ethanol per 1 liter DI water = 1 ppm) mixture of acetone/ethanol with DI water. The air is usually blown inside the flask and later takes out through the outlet to expose the sensor (fig. 2.29a). The atmospheric air already has some water portion that changes the ppm ration. Therefore, another set up has been developed (fig. 2.29b) without incorporation of air blower. In this setup, the sensor is usually kept inside the flask. Unfortunately, still there is a strong possibility that the sensitivity of the sensor will be inaccurate due to the long-time exposure. In spite of that, the sensor was inserted into the chamber after heating the mixture for certain time ($\approx$30 minutes).
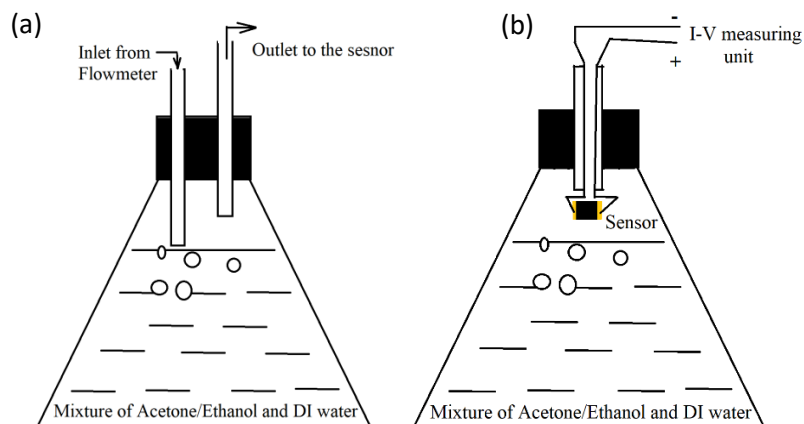
Figure 2.26. Sensitivity measurement unit for ppm concentration.

2.5.9   Four-point probe analysis

Four-point probe is one of the typical and most extensively used gadgets for the measurement of Surface resistivity of a film. It comprises of four tungsten probes, arranged in linear distance (S) in a straight line (fig. 2.27). A constant current is passed through the two

probes with the help of a constant current supply. In the meantime, the potential drop (V) is measured across the middle probes [129].
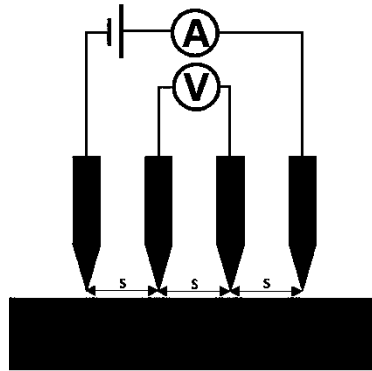
Figure. 2.27. Four-point probe for surface resistivity measurement.

Finally, the surface resistivity is calculated by the equation, $R = \rho \frac{L}{A}$, where $\rho = R \times \frac{A}{L} = \frac{V}{I} \times \frac{A}{L}$.... (15). The ρ is the resistivity (unit - Ω-m) of the conductor.

Chapter 3: Development and fabrication of sensors

3.1 Graphene solution preparation

The graphene solution is prepared by following 3 steps. In the first step, 0.26g nickel chloride ($NiCl_2$), 0.5g Ni nanoparticles, 0.2g polyvinyl pyrrolidone and 1ml hydrogen per oxide (H_2O_2) has been added in a 20ml vial. After one hour, the solution was sonicated for 5 minutes. In the second step, a mixture of 0.02g Poly-(Sodium-p-styrenesulfonate) and 4ml limonene was kept in another vial for one hour and then sonicated for 5 minutes. The function of Ni is to enhance the electron mobility, $NiCl_2$ works as a catalyst, polyvinyl pyrrolidone is as binder for graphene layer to the substrate and H_2O_2 is to increase the oxidation-reduction in the solution. in addition, Poly-(Sodium-p-styrenesulfonate) works as a graphene emulsion Stabilizing polymer and limonene helps to make bonds between insoluble positive and negative portion of the solution.

In the third step, both solutions were added and later sonicated for 1 minute. After 24 hours 0.005g ethanol blended graphene was added to the solution pre-treated 12ml ethanol. Then the whole solution was sonicated for 3 hours, which makes a solution that lasts >24 hours without suspension (fig. 3.1).
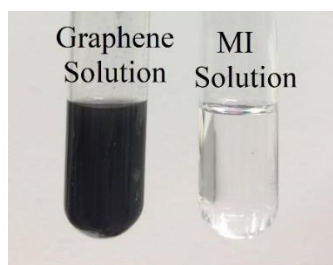
Figure 3.1. Graphene (left) and molecular imprinted (right) solution.

3.2 Gold electrode deposition on substrate

The electrodes of the sensor are deposited on the two sides of the substrate by CrC sputtering (figure 3.2) in vacuum chamber. A patterned mask of thin paper was used to deposit the gold electrodes of 60 nm. While depositing the gold, the middle portion of the substrate

remains unexposed due to the mask pattern. In sputtering technique, the ionized argon atoms are attracted by the cathode and continuously raid on the target material. In the meantime, the target material is sputtered out from the surface and deposited substrate (figure 3.2).
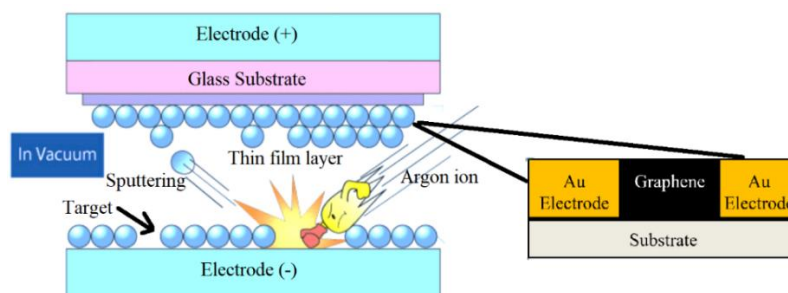
Figure 3.2. Working principle of sputtering[130] and Device configuration with graphene and gold electrode.

3.3   Spray Coating technique

The cost effective and easy spray coating method is being used in this work to fabricate the graphene channel in between the gold electrode. The spray coater sprays the solution by the pressurized nitrogen flow (fig. 3.3a). Here to say that, the particle size in the solution must be very small. Otherwise the sprayr will be blocked. Moreover, the spray coating method needs to maintain specific spray coating distance (between substrate and sprayer – 2 inches), time (3 minutes) and pattern (discussed in result) to fabricate graphene channel. Furthermore, it is not that easy task to fabricate samples (fig. 3.3b) with repeatable parameters like resistance and thickness by using spray coater. Therefore, I-V analysis, four-point probe method and Daktak thickness measurement were done to find the films that have almost same surface resistivity and film thickness.
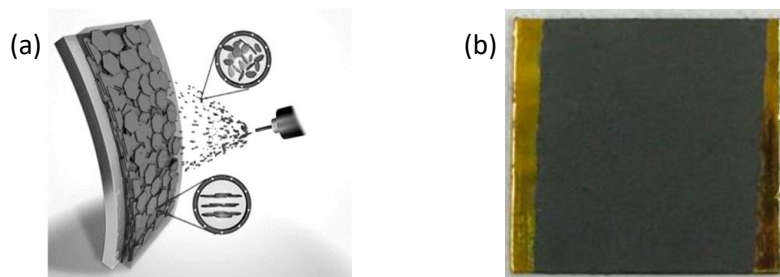
Figure 3.3. a) Spray coating technique[12] and b) fabricated graphene film (0.8×0.8 inch).

3.4 Molecular imprinting layer fabrication

The molecular imprinting layer was fabricated by adding 6ml acetone/ethanol, 0.1g polyethylene glycol (PEG) and 0.1g tin di-oxide (SnO_2) nanofiber. The PEG works as a polymer matrix. The SnO_2 helps to increase the sensitivity and works as a catalyst in the solution. However, acetone or ethanol was used as a template. The solution was sonicated for one hour and later fabricated as imprinted layer over graphene by drop casting method (fig. 3.4).
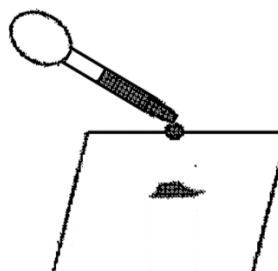
Figure 3.4. Drop casting method.

A maintained heat of 35^0C is usually given to the sample to make the imprinted layer smooth as much as possible. The PEG also fills the defects in the graphene layer and enhances the electron flow in the graphene layer by reducing the trapping of electrons inside the defect. Moreover, the imprinted layer is very thin and transparent (figure 3.5a). Therefore, it is invisible after fabricating over graphene layer (fig. 3.5b). Even, the binding of PEG and rough graphene surface is significantly better, that the flexing of the substrate does not have any effect on the adhesion of the imprinted layer (fig. 3.5c).
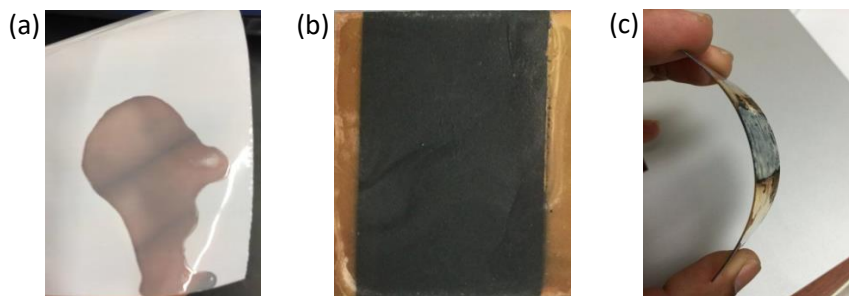
Figure 3.5. (a) MI layer on PE membrane, (b) fabricated graphene on film and (c) bendability.

Moreover, the molecular imprinted layer works as a protective layer for the graphene while sensing. It separates the graphene layer from the ambient weather. Though it permits specific molecules to go through, at the same time, it facilitates the sensor for removing other ambient molecules. It also reduces the interaction of defected graphene layer.

Chapter 4: Result and performance analysis

4.1 SEM analysis of Graphene

The figure 4.1b is showing the reduction of the nanoplatelets flakes size (25µm width – fig. 4.1a) to a few micrometers. It is also considerable that the sonication enhanced the reduction of the flake area. Though, the solution gave suspension after a certain time (40 hours), but then again sonication for 5 minutes helps to regain the solubility of the graphene.
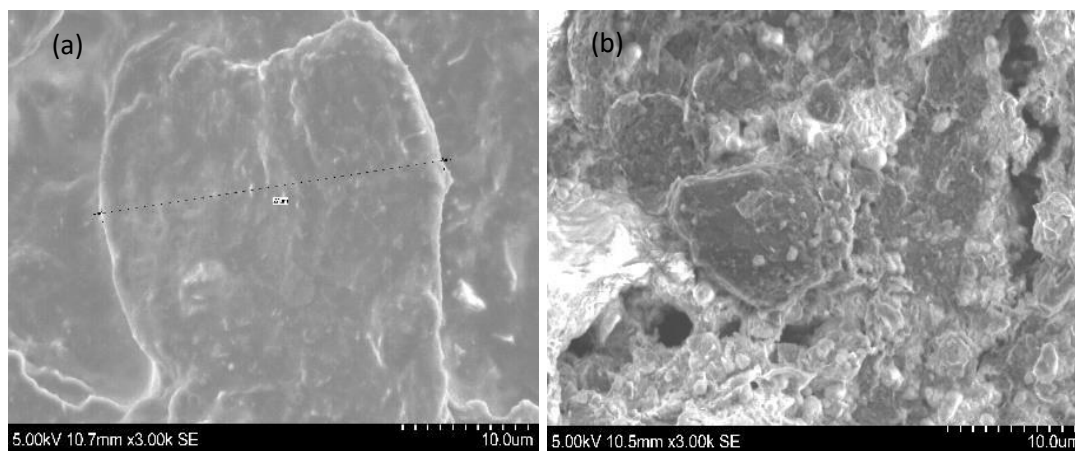
Figure 4.1. SEM of (a) 25µm graphene flakes (b) reduced graphene flakes (sample size 0.8×0.8 inches).

4.2 Optimization of the spray coating pattern of graphene film

There are some special parameters that should be maintained to get good spray coating results. The spray coating pattern, distance between the spray coater and the substrate along with spray coating time are few of them. A specific distance of 2 inches with 3 minutes coting time was maintained to get better film. In addition, a specific spray coating pattern was followed for fabricating the graphene channel in between the gold electrode. The patterns are three types which are a combination of five primary patterns shown below.
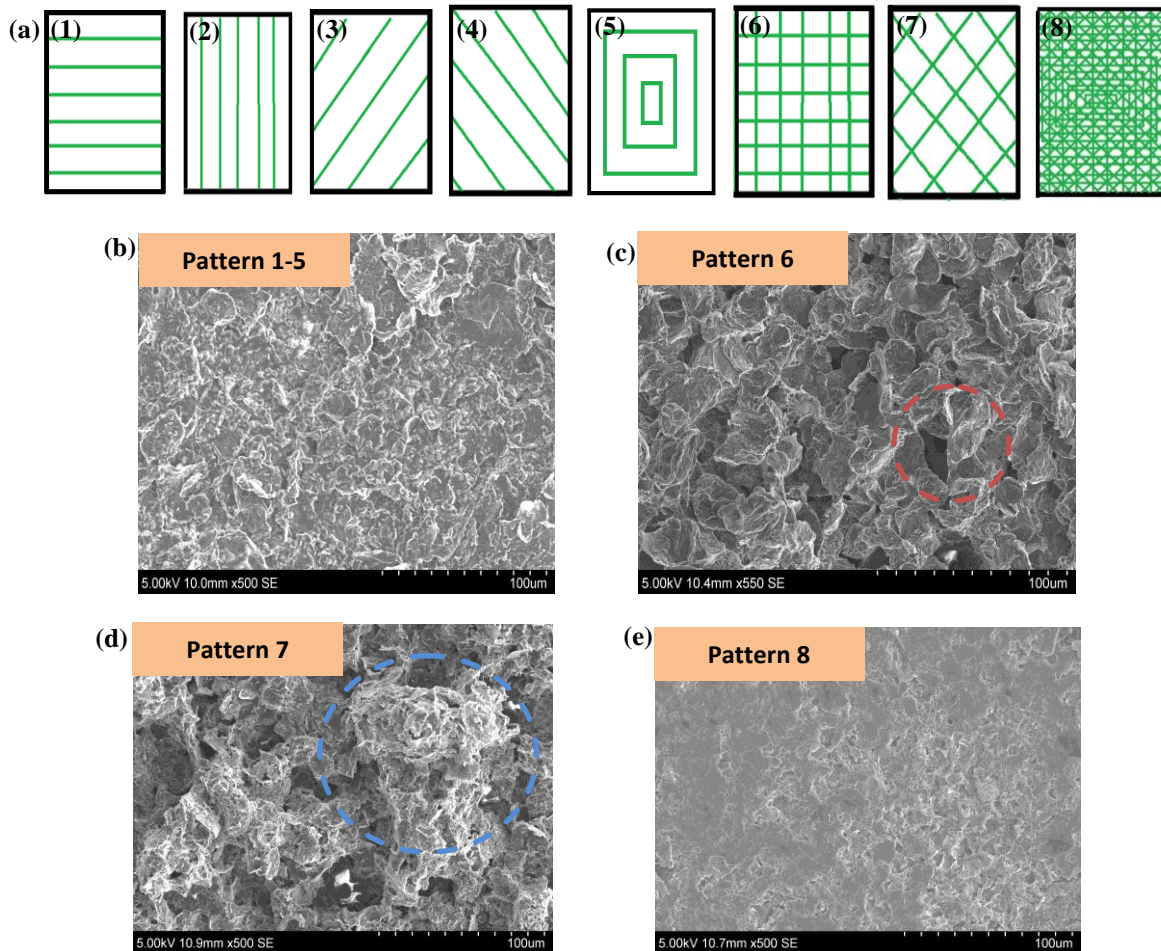
Figure 4.2 (a) Optimized spray coating pattern (1-8), (b) SEM of pattern 1-5, (c) SEM of pattern 6, (d) SEM of pattern 7 and (e) SEM of pattern 8

After following patterns 1-5, the surface of the graphene layer turned out very rough due (fig. 4.2b) to the overlapping of one track of spray coating pattern with another track. Moreover, the flakes attaching was very bad with the substrate. The high roughness resulted into high Surface resistivity in MΩ/GΩ range. A very low resistance from the graphene layer was expected to implement the sensor in low power circuit. The high roughness and poor graphene attaching to the substrate limits that possibility. Thus, patterns 6 and 7 were used. It is found that the layer attaching is still unfortunate. Even, the SEM image of the pattern 6 was demonstrated the pinhole formation (red circle in fig. 4.2b), while the pattern 7 had many towers and pinholes (Blue circles in fig. 4.2c).

Finally, a combined pattern of 5, 6 and 7 was used to create a new pattern 8. The Related SEM image is shown in fig. 4.2d. A very high graphene flakes compaction and less rough surface feature were found. Besides, the lowest graphene layer resistance of 68Ω/sq.m (using four-point probe method) was found in pattern 8 based film. Additionally, after the fabrication of the graphene layer, an annealing temperature of about 60^0 C was used on the substrate for 15 minutes. This is a significant factor to improve the layer formation and crystallization of the graphene.

4.3 Imprinted layer morphology

The smoothness of the imprinted layer on top Graphene is another principal issue for better acetone and ethanol sensing. However, it is expected to have a porous imprinting layer in both acetone and ethanol sensor, where the pores will act like a size based channel to permit acetone and ethanol. Besides, the acetone and ethanol molecule have a very small kinetic diameter (table 2.1). Therefore, the pore size in imprinted layer will be very small (<1nm) eventually. It is not an easy task to characterize pores that's are less than 1nm. The SEM images in figure 4.3a and 4.3b are showing a very smooth topographical contrast of acetone and ethanol imprinted layer.
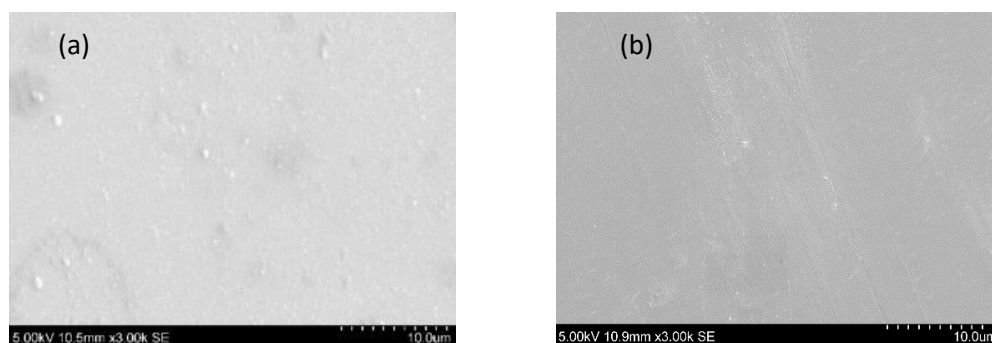
Figure 4.3. SEM image of MI layer morphology (a) acetone sensor and (b) ethanol sensor (sample size 0.8×0.8 inches).

4.4   **Thickness profile of graphene and molecular imprinted films**

The thickness of the graphene layer is 0 to >1 µm for Acetone sensor and 5-6 µm for ethanol sensor. The graphene layer thickness is lower in acetone sensor than the ethanol sensor, because of the very low acetone concentration in breathing. Furthermore, the average thickness or the graphene layer with imprinting layer is 2-3 µm for acetone sensor and 6-8 µm for ethanol sensor (fig. 4.10). The thickness profile was measured by Dektak profilometer (fig. 4.4).
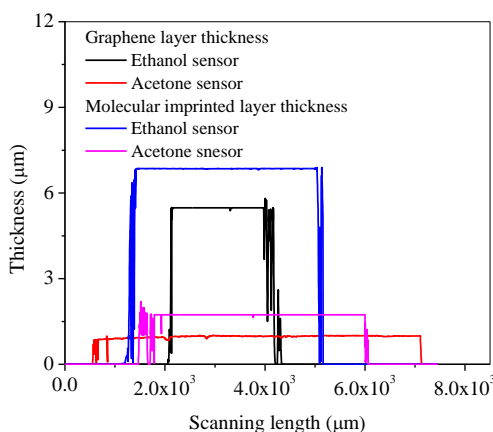
Figure 4.4. Thickness profile of Graphene and MI layer in acetone and ethanol sensor (sample size 0.8×0.8 inches).

4.5   **Raman analysis**

The figure 4.5a is showing the Raman spectrum of fabricated Graphene film where D, G and 2D band is found in 1342.9, 1673.6 and 2704.23 Cm^{-1} respectively. The position of both D and G band shifted to the right due to the sensitivity of the laser to the surrounding environment. In addition, the change in crystal phase, local strain, and degree of crystallinity can shift the Raman peak position. Another peak at 538 cm^{-1} with a very low intensity was found in the Raman spectra for SnO_2 nanofiber. Usually, PEG peak appears in between 1481 – 1486 cm^{-11} [131], but experimental result shows that the peak is split into 1464.5, 1488 and 1495.12 Cm^{-1}. The reason is the fluctuation in the vibrational energy state during experiment [132]. Moreover, the interaction of PEG with acetone and ethanol is another reason for change in peak position (figure 4.5b).
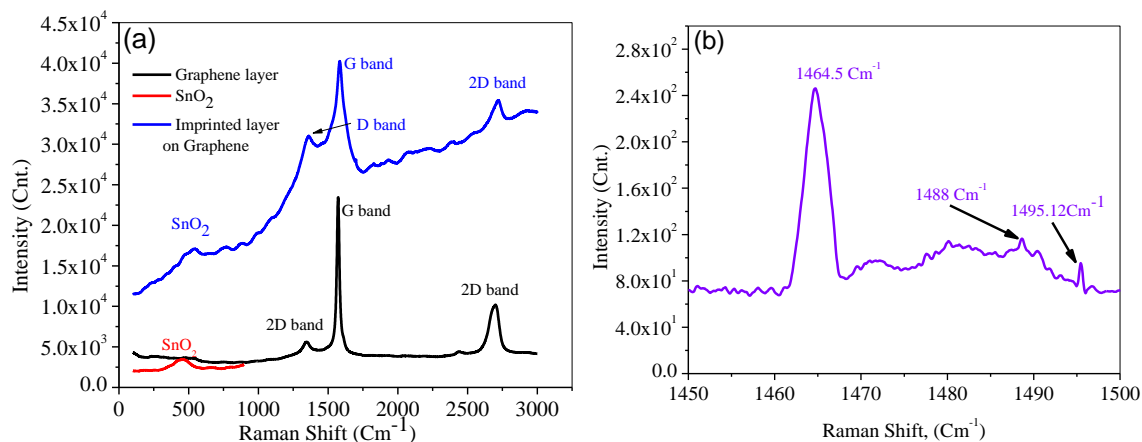
Figure 4.5. Raman spectrum of (a) fabricated sensor and (b) magnified PEG peak (sample size 0.8×0.8 inches).

On the other hand, the annealing temperature influences crystallinity and the homogeneous nature of the film. The Raman analysis is a useful tool to select the proper annealing temperature after fabricating graphene channel. The figure 4.6 shows the Raman analysis of the graphene channel for optimizing the annealing temperature. The 80^0C annealing temperature is exhibited the highest intensity for the G-band. Nevertheless, it is not efficient as optimized temperature due to the 10 minutes annealing time. It has been observed that the substrate starts to bend due to the 80^0C annealing for 15 minutes. Though, the G-band is very low in 70^0C annealing temperature, but D and 2D band are very low comparing to the others. Even, the full width at half maximum (FWHM) of G-band at 70^0C is 25.9 cm^{-1}, Which is smaller than others (80^0C - 35.7 Cm^{-1}, 90^0C - 78.6 Cm^{-1}, 100^0C - 55.56 Cm^{-1})
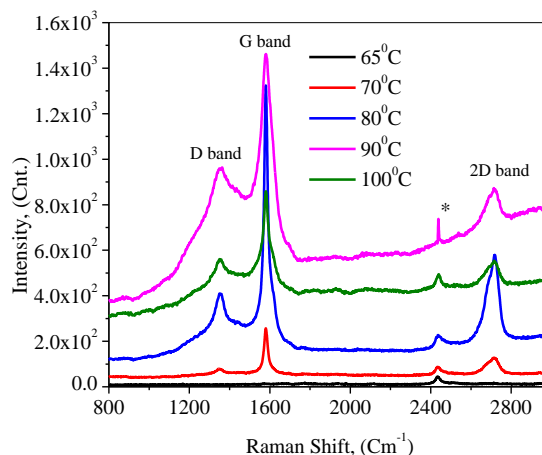
Figure 4.6. Raman peak of related to the annealing temperature optimization (star mark indicating the splitting of the 2D band, which causes due to the temperature and strain effect) (sample size 0.8×0.8 inches).

4.6   ATR-IR analysis of functional group

The figure 4.7 shows the ATR-IR results of the fabricated graphene sample after exposing by ethanol and acetone. The Carbonyl functional group for acetone exposed sensor was found in 1720 cm^{-1}. Moreover, a broad left shifted O-H band was found (3000-3700 cm^{-1}) for ethanol exposed sensor. The shifting was the impact of the C-H band that found in 2850-2975 cm^{-1}. Even for Acetone, a wider C-H bond was found, which is a combination of C-H and O-H functional group.
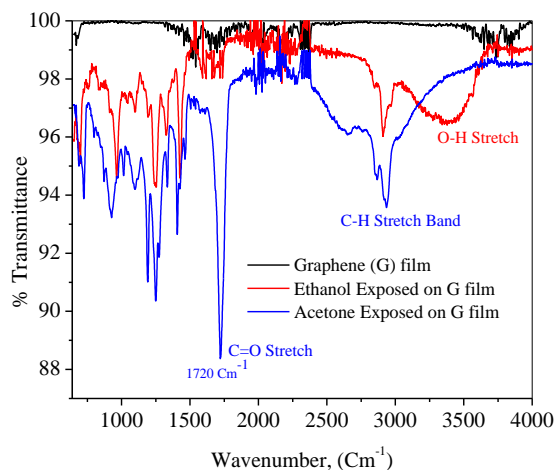
Figure 4.7. ATR-IR analysis of acetone and ethanol exposed sample (sample size 0.8×0.8 inches).

4.7 Selectivity of acetone and ethanol sensor

The imprinted sensors were exposed by acetone and ethanol and the resistance change was observed by following the Rotameter based measurement. In case of acetone imprinted sensor, the resistance was increased from 222.22Ω (100 cc/min) to 320.51Ω (400 cc/min) with significant linear characteristics (figure 4.8a). Same characteristic was also observed in the ethanol imprinted sensor (figure 4.8b) and resistance was changed from 200.35 Ω (100 cc/min) to 376.18 Ω (400 cc/min).
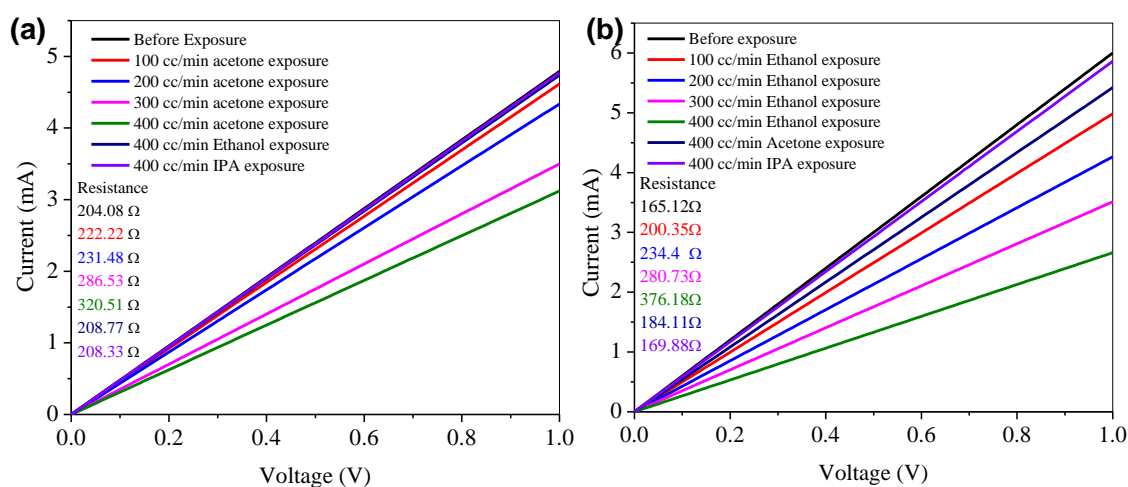
Figure 4.8. Acetone and ethanol selectivity of graphene with MI layer (sample size 0.8×0.8 inches).

Yet, in the acetone and ethanol imprinted sensors, there are slight sensitivity for the other molecules (fig. 4.8 - resistance value). It is due to the defects in the imprinted layer, molecular kinetic diameter mismatch with the pore of the filter and measurement errors. Moreover, the water molecule has a smaller kinetic diameter than acetone, ethanol or IPA. Therefore, it will always affect the selectivity. The figure 4.9a and 4.9b shows the sensitivity of the sensor to the dry (relative humidity - 5.52% and dew point – 1^0 F) and wet air (relative humidity- 90% and dew point 69^0 F). The variation of current level (or resistance change – Table 4.1) is very small, which refers to the fact that the sensors are very less responsive to the water molecule.
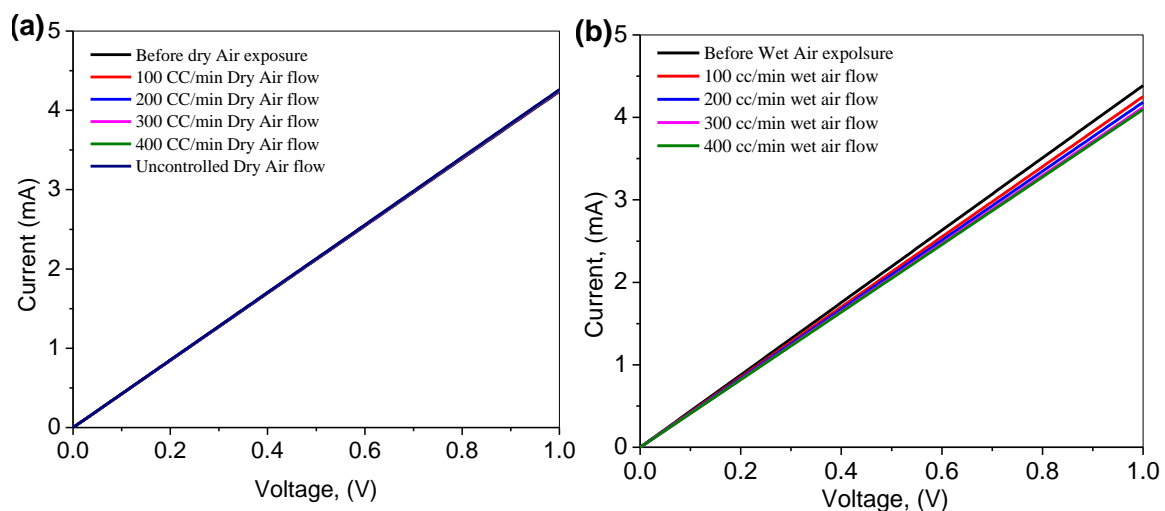
Figure 4.9. Dry (a) and wet (b) air sensitivity of graphene film with MI layer (sample size 0.8×0.8 inches).

Table 4.1. Resistance change while exposing dry and wet air.

Exposure cc/min	Resistance (Ω)	Resistance (Ω)
	Dry Air	Wet air
0	235.89	235.84
100	235.875	237.79
200	235.874	238.31
300	235.859	238.83
400	235.84	240.41

4.8 Sensitivity of the acetone and ethanol sensor – (ppm scale)

The acetone imprinted sensor was exposed by 0-10 ppm acetone vapor and the figure 4.10a shows the current sensitivity. Figure 4.10b shows the resistance sensitivity of the acetone imprinted sensor.
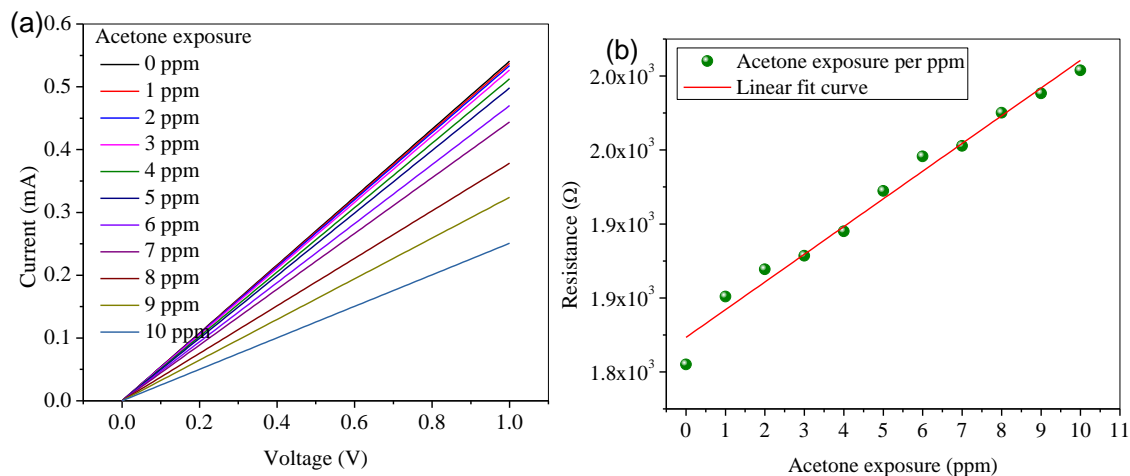
Figure 4.10. (a) Current sensitivity and (b) sensitivity of acetone imprinted sensor per ppm acetone (sample size 0.8×0.8 inches).

The current flow through the graphene layer was decreased while the exposure amount increased. It was happened due to the increasing of the resistance of graphene layer (table 4.2).

Table 4.2. Resistance change with respect to acetone exposure per ppm.

Acetone exposure (ppm)	Resistance change (Ω)
0	1805
1	1850.88
2	1869.35
3	1878.5
4	1895
5	1922.371
6	1945.63
7	1952.1
8	1975.2
9	1988.25
10	2003.77

The Sensitivity of the sensor was calculated by using the data presented in the table 4.2.

Acetone sensitivity of the sensor =

$$\frac{\text{Resistance at 10 ppm Acetone exposure} - \text{Resistance at 0 ppm Acetone exposure}}{10 \text{ ppm} - 0 \text{ ppm}}$$

$$= \frac{2003.77 - 1805}{10}$$

$$= 19.877 \ \Omega/\text{ppm}.$$

The exposure time is a very important factor in sensor characteristics. Figure 4.11 shows the clear validation of the importance of the exposure time. It has been observed that the sensor characteristic was nonlinear while exposure time is more than 10 second. In contrast to that, the acetone sensitivity is linear for 3 second exposure. The concentration of the acetone molecule is very small and available adsorption sites in the graphene layer are huge. That's why the adsorption dynamics in 3 second exposure is following Langmuir model. However, the liner characteristics of the curve changed to Freundlich ($n>1$) or Langmuir ($R_L>1$) model for 10 second exposure. The Freundlich ($n>1$) or Langmuir ($R_L>1$) are highly unfavorable due to the high separation factor (R_L). This high separation factor decreases the desorption of adsorbate by increasing the intermolecular interaction. That means the long-time exposure decreases the possibility of the desorption from the absorbent [133]. Therefore, in long time exposure, the molecules are used to stay on the adsorbent for long time and increases the resistance abruptly.
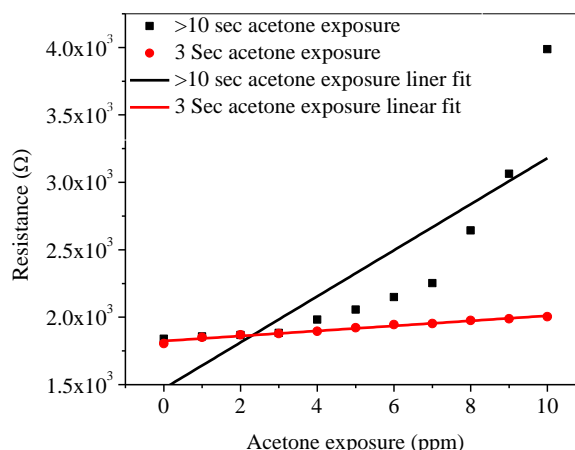
Figure 4.11. Optimization of exposure time (sample size 0.8×0.8 inches).

The optimized 3 second exposure time was also used for the ethanol sensor. The characteristic of the curve was linear in 130 – 280 ppm range of ethanol exposure. The resistance of the film went too high (table 4.3) and consequently the current level went down beyond this

range. The current level change with the increasing ethanol concentration is shown in the figure 4.12.
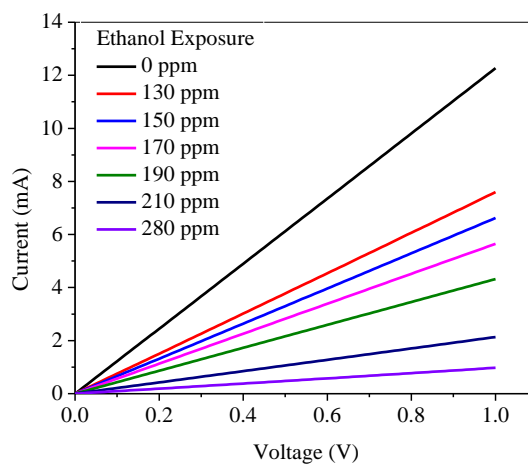
Figure 4.12. Ethanol sensitivity of ethanol imprinted sensor per ppm (shown in 10 ppm interval for clear view).

Table 4.3. Resistance change as a function of ethanol exposure.

Ethanol Exposure (ppm)	Resistance change	Ethanol Exposure (ppm)	Resistance change	Ethanol Exposure (ppm)	Resistance change
130	148.5	190	329.86	250	789.8
135	152.11	195	348.19	255	838.76
140	166.9	200	367.52	260	860.2
145	184	205	414.5	265	891.5
150	207.7	210	435	270	945.7
155	222.19	215	447.9	275	964.12
160	241.6	220	479.13	280	1024.19
165	257	225	543.6	285	1028.73
170	269.3	230	595.33	290	1030.5
175	282.77	235	662.75	295	1031.754
180	291.2	240	698.3	300	1033.44
185	312.11	245	760.6		

The figure 4.13 shows the resistance characteristic of the ethanol sensor. At first the monolayer formation of the adsorbate started and the curve increased linearly. After 215 ppm exposure, the resistance started to increase drastically due to the multilayer adsorbate formation

as well as intermolecular interaction. Finally, the curve was saturated (>280 ppm of ethanol exposure). Therefore, the ethanol sensitivity curve is a BET model based curve.
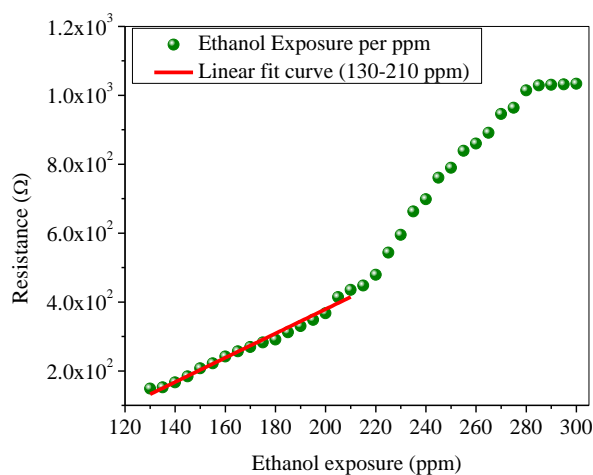
Figure 4.13. Ethanol sensitivity per ppm (sample size 0.8×0.8 inches).

Finally, the Sensitivity of the ethanol sensor was calculated by using the data of the table 4.3.

$$\text{Ethanol Sensitivity} = \frac{\text{Resistance at 210 ppm ethanol exposure} - \text{Resistance at 130 ppm ethanol exposure}}{210 \text{ ppm} - 130 \text{ ppm}}$$

$$= \frac{435 - 148.5}{80}$$

$$= 3.58 \ \Omega/\text{ppm}.$$

4.9   LOD Analysis – Acetone and Ethanol sensor

The LOD of the acetone sensor was calculated 0.26 ppm by using the equation 9, 10 and 11. This is below the lowest acetone breath amount in completely healthy persons (0.32 ppm). It is only an estimated value. The LOD for the ethanol sensor was found 78.76 ppm (using 130 – 210 ppm range values). The LOD of acetone sensor (0.26 ppm) could not be measured practically because of the unavailability of existing frameworks. Table 4.4 is showing the resistance change below 130 ppm. The resistance of the sensor was very amall below 100 ppm (table 4.4) and after 78 ppm it was almost same.

Table 4.4. Resistance change of the ethanol sensor below 130 ppm.

ppm	Resistance change
130	143.84
120	141. 22
110	137.2
100	135.19
90	135.1
80	134.8
70	134.29

4.10   Gas response and percentage sensitivity of acetone and ethanol sensor

The gas response and percentage sensitivity were calculated by equation 7 and 8. Figure

4.14 shows the gas response and percentage sensitivity for both acetone and ethanol sensor.
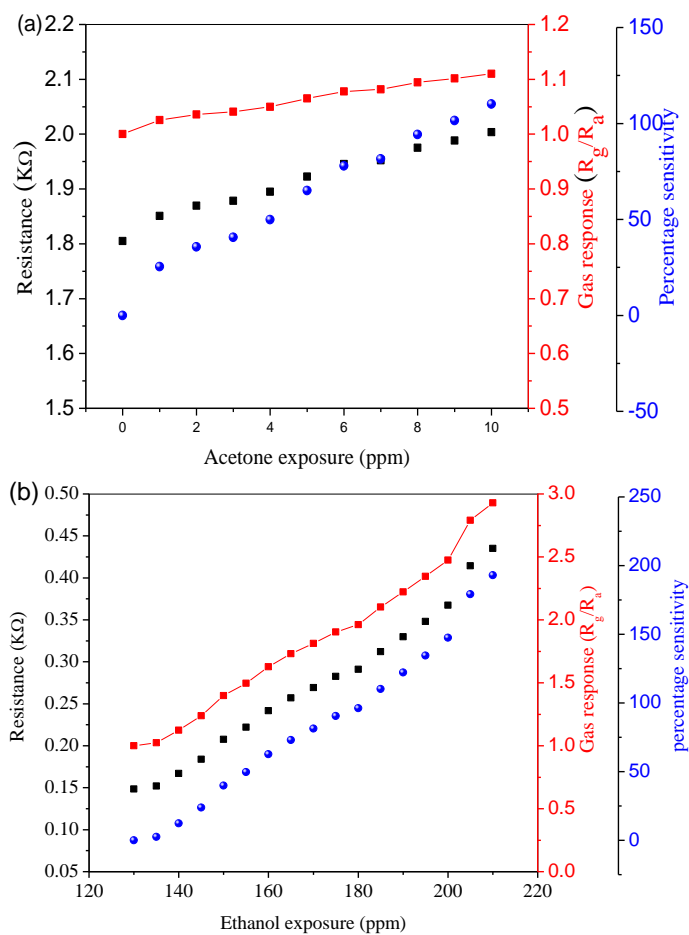
Figure 4.14. Gas response (a) and percentage sensitivity (b) of acetone and ethanol sensor (sample size 0.8×0.8 inches).

In both cases, the gas response and percentage sensitivity was increased with the increase of the exposure concentration and resistance of the graphene film. In case of acetone imprinted sensor, the gas response R_g/R_a was 1.1 with maximum 2.16 for best sample. In case of ethanol imprinted sensor, the gas response R_g/R_a was ≈3 with maximum 4.16 for best sample. The maximum percentage sensitivity of the sensors was increased 111% for acetone sensor and 192% for ethanol sensor.

4.11   Repeatability

The repeatability of the acetone sensor was evaluated by exposing 8 sensors of same sheet resistance (≈95 Ω/sq.m) in the range of 0 -10 ppm of acetone. Figure 4.15a shows the sensitivity of 8 acetone imprinted sensors and fig. 4.15b shoes the value of the sensitivity, which are relatively same.
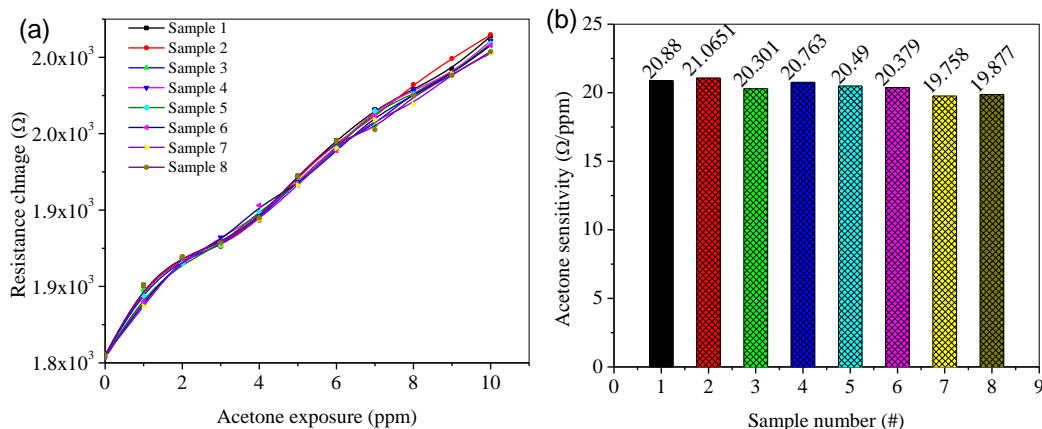
Figure 4.15. (a) Acetone sensitivity of 8 samples and (b) Repeatability of acetone sensor (sample size 0.8×0.8 inches).

Even, the calculated ML and WLS value (using eq. 12 and 13) between the sensors that have maximum and minimum sensitivity was about 0.003, which is very small. Therefore, the maximum deviation of the sensitivity between the acetone sensors remained same with average sensitivity of 20.4 Ω/ppm acetone. Moreover, the slope difference between the I-V curve of the sample that has maximum and minimum sensitivity is 0.9792 (fig. 4.16) with relatively same r^2 value.
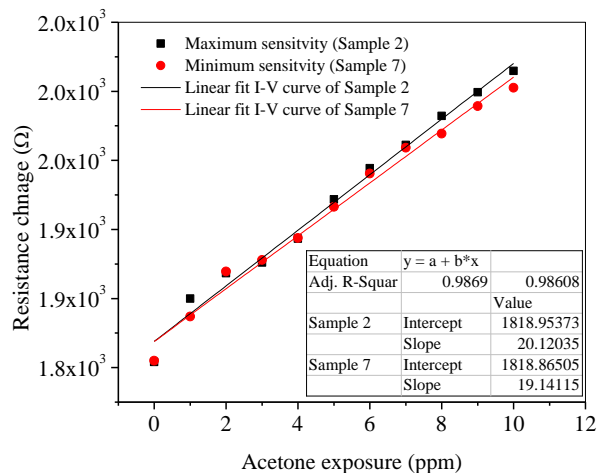
Figure 4.16. Deviation comparison bet en maximum and minimum acetone sensitive sample.

In case of ethanol sensor, the average sensitivity of the 8 samples was calculated around 3.74 Ω/ppm ethanol. The sensitivity curve (fig. 4.17a) along with the value (fig. 4.17b) of those 8 samples is shown in figure 4.24.
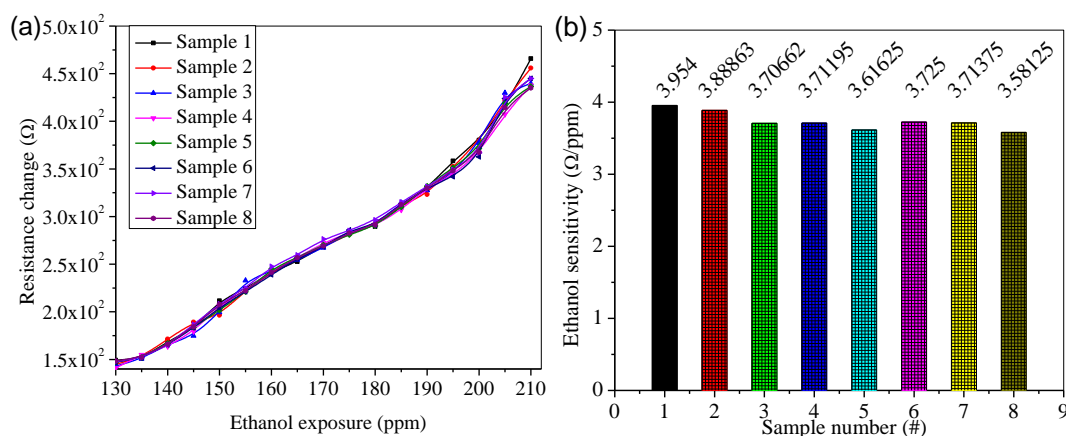
Figure 4.17. (a) Ethanol sensitivity of 8 samples and (b) Repeatability of ethanol sensor (sample size 0.8×0.8 inches).

The ML and WLS value (using eq. 12 and 13) between the sensors that have maximum (sample 1) and minimum (sample 8) sensitivity was about 0.013289217 and 0.013693472 respectively which are relatively same and small. In addition, the slope difference between the I-V curve of both samples was 0.1681 (fig. 4.18) with relatively same r^2 value. Therefore, the repeatability for the ethanol sensors was very good.
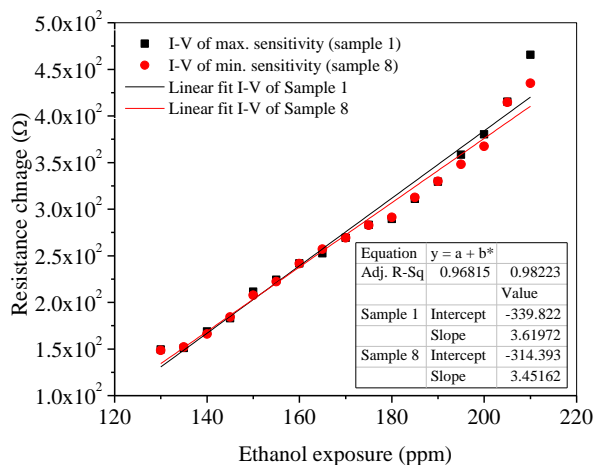
Figure 4.18. Deviation comparison between maximum and minimum ethanol sensitive sample.

4.12   Stability

The stability of the sensor has been observed for 32 days. Figure 4.19 shows the stability of the sensor as a function of percentage stability change and resistance change (using eq. 14) [134]. The sensors were exposed in controlled amount of acetone and ethanol (ppm scale) every time during the test (verified by commercial acetone (MQ-138) and ethanol sensor (MQ-8)). The measurement was done in the ambient atmosphere. Rest of the time they were sealed in a sample box. Every day the samples were also investigated by Raman analysis to check the quality of graphene and imprinted layer.
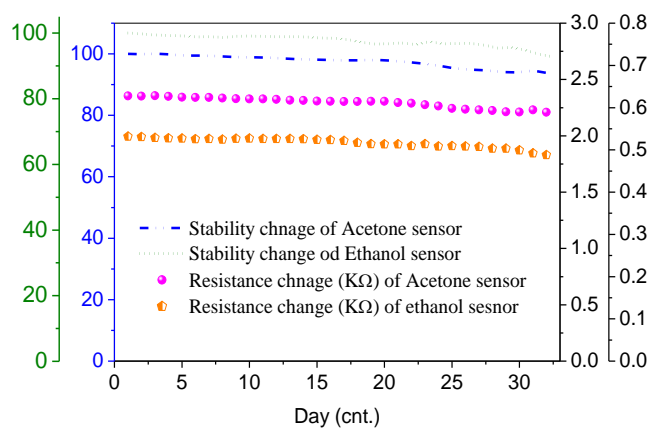
Figure 4.19. Stability and resistance change of acetone and ethanol sensor for 32 days (sample size 0.8×0.8 inches).

In acetone sensor, the resistance sensitivity was decreased about 6.2% (for 10 ppm acetone) after 32 days. In case of ethanol, the resistance sensitivity was decreased about 8.2% (for 210 ppm ethanol) after 32 days. Moreover, the stability of the acetone and ethanol sensor was more than 90%. A minor stability loss was observed due to the thickeners variation, ambient temperature effect along with molecular interaction during the experiments and measurement errors.

Chapter 5: Conclusion

5.1 Summary of the work

Recently, the diabetes and alcohol care plan are now more oriented in earlier detection rather than lab based diagnosis. The Point of Care Testing (POCT) device for diabetes and alcohol detection is a very reliable solution for on-site detection. However, developing a breathing sensor is not always an easy task due to the complex molecular science. An ideal breathing sensor requires uniform detection, selective sensing, suitable conductivity and higher chemical. Some of the existing acetone sensors have selective sensitivity only under controlled environment and a huge portion of alcohol sensor is based on complex detection systems. So, it is very necessary to develop a low cost, selective and stable sensor that can detect alcohol and ethanol without suffering by the ambient environment. An efficient imprinting technique can improve the selectivity of the sensor, where the imprinting layer usually filters the ambient molecules and only permits specific molecules to go through. In this work the imprinting layer was consisted by PEG and SnO_2 nanofiber that increases the conductivity while sensing. However, previously reported acetone and ethanol sensor never used imprinting technique, which enables the nobility of this work. The making of graphene and imprinting layer solutions along with their fabrications are very simple. Several simple characterizations (Raman, SEM and ATR-IR) along with I-V analysis have been explored to understand the sensing mechanism and criteria of the sensors. The material quality, sensing repeatability and stability was also described with proper explanation. Finally, molecular imprinted acetone and ethanol sensor were developed with optimized graphene and imprinting layer thickness.

5.2   Conclusions

A novel molecular imprinted acetone and ethanol sensor was developed to detect diabetic and alcoholic patients conveniently. The designed sensors can detect 0 -10 ppm acetone concentration with a highest sensitivity of about 21.06 Ω/ppm and 130 - 208 ppm ethanol concentration with a highest sensitivity of about 3.58 Ω/ppm. The response time was 3 second with 20 – 40 second recovery time for both sensors. Moreover, the acetone sensitivity was liner in 0-10 ppm of acetone concentration. On the other hand, ethanol imprinted sensor had linear increasing characteristic in 130-210 ppm of ethanol concentration (permissible alcohol range). The highest acetone response (R_g/R_a) was found 1.1 for 3 second exposure with 2.16 for best sample. In case of the ethanol imprinted sensor, it was about 3 and ~5 for best sample. The calculated lowest limit of detection for acetone sensor was 0.26 ppm and 78.76 ppm for ethanol sensor.

Furthermore, the developed sensors are reliable (90-95%) for a long time (>32 days). In contrast of that, most of the commercial sensors are efficient in real time measurement due to the moisture, CO_2 and other kind of air particle interaction. The designed sensors were very efficient in the ambient environment and all the characterizations were done in ambient environment as well. The repeatability of the sensors were very good with low value of ML, WLS and slope difference. The parameter like current and resistance change of the designed sensors are very easy to use as a detection parameter. They are also very enticing for portable sensing device application. Finally, the sensitivity, reliability and stability of the sensors are very significant within a wide detection range comparing to the commercial sensors. Therefore, the sensor developed by following this work will be an easy choice to commercialize for both home and clinical user.

5.3   Future works

This work can be modified by using transistor configuration with optimized imprinting technique for small transistor channel. Nevertheless, the design and development of breathing monitor device, electric circuit with real time tracking and feedback capacities can be an extension of this work. In addition, the noise of the transistor devices may alter due to the different acetone or ethanol concentration. The linear regression technique can be used to fit the noise spectrum to get another novel optimized sensitivity parameters. Moreover, the future goal can be introduced as wrist band or small gun shape device with smart LED indication (such as red = dangerous level, yellow =near danger, green = ok and blue = low amount of acetone or ethanol) or alarm system (fig. 5.1) to make it more user friendly. Finally, machine learning and computational intelligence can be espoused to develop a smart phone or computer based real-time breath tracking system.
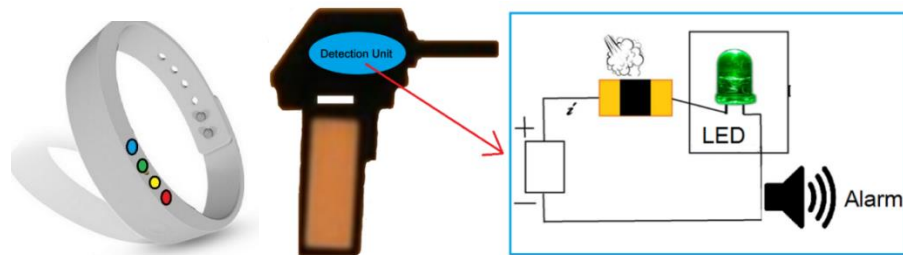
Figure 5.1. Device configuration and circuit connection for future product.

References:

1. Choi, W., N. Choudhary, G.H. Han, J. Park, D. Akinwande, and Y.H. Lee, *Recent development of two-dimensional transition metal dichalcogenides and their applications.* Materials Today, 2017.

2. Xia, F., H. Wang, D. Xiao, M. Dubey, and A. Ramasubramaniam, *Two-dimensional material nanophotonics.* Nature Photonics, 2014. **8**(12): p. 899-907.

3. Yang, J.C., H.-K. Shin, S.W. Hong, and J.Y. Park, *Lithographically patterned molecularly imprinted polymer for gravimetric detection of trace atrazine.* Sensors and Actuators B: Chemical, 2015. **216**: p. 476-481.

4. Ertürk, G., H. Özen, M.A. Tümer, B. Mattiasson, and A. Denizli, *Microcontact imprinting based surface plasmon resonance (SPR) biosensor for real-time and ultrasensitive detection of prostate specific antigen (PSA) from clinical samples.* Sensors and Actuators B: Chemical, 2016. **224**: p. 823-832.

5. Lu, C.-H., Y. Zhang, S.-F. Tang, Z.-B. Fang, H.-H. Yang, X. Chen, and G.-N. Chen, *Sensing HIV related protein using epitope imprinted hydrophilic polymer coated quartz crystal microbalance.* Biosensors and Bioelectronics, 2012. **31**(1): p. 439-444.

6. Moxfyre. *Molecular energy levels and Raman effect*. 2009 04/26/2016 [cited 2017 05/24/2017]; Available from: https://commons.wikimedia.org/wiki/File:Raman_energy_levels.svg#mw-jump-to-license.

7. Karl Sandeman (Imperial College, L. *Raman Spectroscopy*. 2007 [cited 2017 05/24/2017]; Available from: https://www.doitpoms.ac.uk/tlplib/raman/printall.php.

8. Malard, L., M. Pimenta, G. Dresselhaus, and M. Dresselhaus, *Raman spectroscopy in graphene.* Physics Reports, 2009. **473**(5): p. 51-87.

9. Gable, K. *FTIR Spectroscopy*. Fourier Transform Infrared 2013 [cited 2017 05/24/ 2017]; Available from: https://chemistry.oregonstate.edu/courses/ch361-464/ch362/irinstrs.htm.

10. Milosevic, M., *Internal reflection and ATR spectroscopy*. Vol. 262. 2012: John Wiley & Sons.

11. Winter, A., *Organic Chemistry I 2nd Edition*. For Dummies, ed. A. Winter. 2016, WorldCat: Hoboken, NJ : John Wiley & Sons, Inc., 2014.

12. AZoNano. *Nanoplatelet Surface Coating Applied Using a Spray Gun Spontaneously Self-Assembles into Nano-Walls*. Nanomaterials - Nanotechnology - Featured Articles 2014 [cited 2017 05/27/2017]; Available from: http://www.azonano.com/news.aspx?newsID=29880.

13. Park, J.-K., H.-J. Yee, K.S. Lee, W.-Y. Lee, M.-C. Shin, T.-H. Kim, and S.-R. Kim, *Determination of breath alcohol using a differential-type amperometric biosensor based on alcohol dehydrogenase.* Analytica chimica acta, 1999. **390**(1): p. 83-91.

14. Henry, W., *Experiments on the quantity of gases absorbed by water, at different temperatures, and under different pressures.* Philosophical Transactions of the Royal Society of London, 1803. **93**: p. 29-276.

15. Liebig, J., *Ueber die Producte der Oxydation des Alkohols.* European Journal of Organic Chemistry, 1835. **14**(2): p. 133-167.

16. Anstie, F.E., *Prognosis and treatment of certain acute diseases.* The Lancet, Sept, 1867. **28**(1867): p. 385-387.

17. Cushny, A.R., *The action of atropine, pilocarpine and physostigmine.* The Journal of physiology, 1910. **41**(3-4): p. 233.

18. Bogen, E., *The diagnosis of drunkenness—A quantitative study of acute alcoholic intoxication.* California and western medicine, 1927. **26**(6): p. 778.

19. McNally, W.D., H. Embree, and C. Rust, *ALCOHOLIC CONTENT OF NORMAL PLACENTAL TISSUE.* Journal of Biological Chemistry, 1927. **74**(1): p. 219-222.

20. Harger, R., *Science news.* Science, 1931. **73**(10).

21. Jetter, W., M. Moore, and G. Forrester, *Studies in Alcohol. IV. A New Method for the Determination of Breath Alcohol.* Amer. J. clin. Path., 1941. **5**: p. 75.

22. Greenberg, L.A. and F.W. Keator, *A portable automatic apparatus for the indirect determination of the concentration of alcohol in the blood.* Quart. J. Stud. Alc, 1941. **2**: p. 57.

23. Borkenstein, R., *Breath tests to determine alcoholic influence.* Indiana State Police Manual, 1956.

24. *Apparatus for sampling the human breath*. 1957, Google Patents.

25. Penton, J. and M. Forrester. *A gas chromatographic breath analysis system with provisions for storage and delayed analysis of samples*. in *Proceedings of 5th International Conference on Alcohol and Traffic Safety*. 1969.

26. Bay, H., K. Blurton, H. Lieb, and H. Oswin, *Electrochemical measurements of blood alcohol levels.* Nature, 1972. **240**: p. 52-53.

27. Giffin, C. and L. Sieradski, *Portable mass spectrometer.* 1977.

28. Jarrett, R., H. Keen, and C. Hardwick, *"Instant" blood sugar measurement using Dextrostix and a reflectance meter.* Diabetes, 1970. **19**(10): p. 724-726.

29. Health, U.S.N.I.o. *Diabetes Control and Complications Trial (DCCT)*. 2016 03/16/2016 [cited 2017 05/18/2017]; Available from: http://www.webmd.com/diabetes/control-complications-trial#1.

30. Foundation, D.D. *Diabetes History*. 2014 01/22/2014 [cited 2017 05/18/2017]; Available from: http://www.defeatdiabetes.org/diabetes-history/.

31. Wigmore, J.G. and C.J. House, *Forensic Breath and Blood Alcohol Testing: Past, Present and Future.*

32. Jalal, A.H., Y. Umasankar, P.J. Gonzalez, A. Alfonso, and S. Bhansali, *Multimodal technique to eliminate humidity interference for specific detection of ethanol.* Biosensors and Bioelectronics, 2017. **87**: p. 522-530.

33. Bhuiyan, M.S.A., *2D material in sensor application*, in *Thin film and plasma processing*, D.A. Dubey, Editor. 2017, South Dakota State University: South Dakota State University. p. 1-41.

34. Liu, J., Y. Sun, and X. Fan, *Highly versatile fiber-based optical Fabry-Pérot gas sensor.* Optics express, 2009. **17**(4): p. 2731-2738.

35. Sun, Y., J. Liu, G. Frye-Mason, A. Thompson, S.-J. Ja, and X. Fan. *Development of optofluidic ring resonator based chemical vapor sensing platform*. in *SPIE Defense, Security, and Sensing*. 2009. International Society for Optics and Photonics.

36. Song, X., Z. Wang, Y. Liu, C. Wang, and L. Li, *A highly sensitive ethanol sensor based on mesoporous ZnO–SnO2 nanofibers.* Nanotechnology, 2009. **20**(7): p. 075501.

37. Shin, J., S.J. Choi, I. Lee, D.Y. Youn, C.O. Park, J.H. Lee, H.L. Tuller, and I.D. Kim, *Thin-wall assembled SnO2 fibers functionalized by catalytic Pt nanoparticles and their superior exhaled-breath-sensing properties for the diagnosis of diabetes.* Advanced Functional Materials, 2013. **23**(19): p. 2357-2367.

38. Latif, U. and F.L. Dickert, *Graphene hybrid materials in gas sensing applications.* Sensors, 2015. **15**(12): p. 30504-30524.

39. He, Q., S. Wu, Z. Yin, and H. Zhang, *Graphene-based electronic sensors.* Chemical Science, 2012. **3**(6): p. 1764-1772.

40. Viswanathan, S., T.N. Narayanan, K. Aran, K.D. Fink, J. Paredes, P.M. Ajayan, S. Filipek, P. Miszta, H.C. Tekin, and F. Inci, *Graphene–protein field effect biosensors: glucose sensing.* Materials Today, 2015. **18**(9): p. 513-522.

41. Singh, A., M. Uddin, T. Sudarshan, and G. Koley, *Tunable Reverse-Biased Graphene/Silicon Heterojunction Schottky Diode Sensor.* Small, 2014. **10**(8): p. 1555-1565.

42. Leem, J., M.C. Wang, P. Kang, and S. Nam, *Mechanically self-assembled, three-dimensional graphene–gold hybrid nanostructures for advanced nanoplasmonic sensors.* Nano letters, 2015. **15**(11): p. 7684-7690.

43. Rastgou, A., H. Soleymanabadi, and A. Bodaghi, *DNA sequencing by borophene nanosheet via an electronic response: A theoretical study.* Microelectronic Engineering, 2017. **169**: p. 9-15.

44. Kootenaei, A.S. and G. Ansari, *B 36 borophene as an electronic sensor for formaldehyde: Quantum chemical analysis.* Physics Letters A, 2016. **380**(34): p. 2664-2668.

45. Abbas, A.N., B. Liu, L. Chen, Y. Ma, S. Cong, N. Aroonyadet, M. Köpf, T. Nilges, and C. Zhou, *Black phosphorus gas sensors.* ACS nano, 2015. **9**(5): p. 5618-5624.

46. Cui, S., H. Pu, S.A. Wells, Z. Wen, S. Mao, J. Chang, M.C. Hersam, and J. Chen, *Ultrahigh sensitivity and layer-dependent sensing performance of phosphorene-based gas sensors.* Nature communications, 2015. **6**.

47. Wang, G., R. Pandey, and S.P. Karna, *Phosphorene oxide: stability and electronic properties of a novel two-dimensional material.* Nanoscale, 2015. **7**(2): p. 524-531.

48. Liu, H., A.T. Neal, Z. Zhu, Z. Luo, X. Xu, D. Tománek, and D.Y. Peide, *Phosphorene: an unexplored 2D semiconductor with a high hole mobility.* 2014.

49. Tan, C., P. Yu, Y. Hu, J. Chen, Y. Huang, Y. Cai, Z. Luo, B. Li, Q. Lu, and L. Wang, *High-yield exfoliation of ultrathin two-dimensional ternary chalcogenide nanosheets for highly sensitive and selective fluorescence DNA sensors.* Journal of the American Chemical Society, 2015. **137**(32): p. 10430-10436.

50. Lv, J., S. Zhao, S. Wu, and Z. Wang, *Upconversion nanoparticles grafted molybdenum disulfide nanosheets platform for microcystin-LR sensing.* Biosensors and Bioelectronics, 2017. **90**: p. 203-209.

51. Cheng, M., X. Zhang, M. Wang, H. Huang, and J. Ma, *A facile electrochemical sensor based on well-dispersed graphene-molybdenum disulfide modified electrode for highly sensitive detection of dopamine.* Journal of Electroanalytical Chemistry, 2017. **786**: p. 1-7.

52. Li, X. and X. Du, *Molybdenum disulfide nanosheets supported Au-Pd bimetallic nanoparticles for non-enzymatic electrochemical sensing of hydrogen peroxide and glucose.* Sensors and Actuators B: Chemical, 2017. **239**: p. 536-543.

53. Zhang, D., C. Jiang, and Y.e. Sun, *Room-temperature high-performance ammonia gas sensor based on layer-by-layer self-assembled molybdenum disulfide/zinc oxide nanocomposite film.* Journal of Alloys and Compounds, 2017. **698**: p. 476-483.

54. da Silveira Firmiano, E.G., A.C. Rabelo, C.J. Dalmaschio, A.N. Pinheiro, E.C. Pereira, W.H. Schreiner, and E.R. Leite, *Supercapacitor electrodes obtained by directly bonding 2D MoS2 on reduced graphene oxide.* Advanced Energy Materials, 2014. **4**(6).

55. Gilbert, S.M., G. Dunn, T. Pham, B. Shevitski, E. Dimitrov, S. Aloni, and A. Zettl, *Fabrication of Atomically Precise Nanopores in Hexagonal Boron Nitride.* arXiv preprint arXiv:1702.01220, 2017.

56.   Ahmed, K., R. Dahal, A. Weltz, J.J.-Q. Lu, Y. Danon, and I.B. Bhat, *Metalorganic chemical vapor deposition of hexagonal boron nitride on (001) sapphire substrates for thermal neutron detector applications.* Vacuum, 2017. **137**: p. 81-84.

57.   Jiang, H. and J.Y. Lin, *Review—hexagonal boron nitride epilayers: Growth, optical properties and device applications.* ECS Journal of Solid State Science and Technology, 2017. **6**(2): p. Q3012-Q3021.

58.   Liu, H., C. Duan, C. Yang, W. Shen, F. Wang, and Z. Zhu, *A novel nitrite biosensor based on the direct electrochemistry of hemoglobin immobilized on MXene-Ti 3 C 2.* Sensors and Actuators B: Chemical, 2015. **218**: p. 60-66.

59.   Miranda, A., F. de Santiago, L. Pérez, and M. Cruz-Irisson, *Silicon nanowires as potential gas sensors: A density functional study.* Sensors and Actuators B: Chemical, 2017. **242**: p. 1246-1250.

60.   Dong, H., L. Wang, L. Zhou, T. Hou, and Y. Li, *Theoretical investigations on novel SiC 5 siligraphene as gas sensor for air pollutants.* Carbon, 2017. **113**: p. 114-121.

61.   Feng, J.-w., Y.-j. Liu, H.-x. Wang, J.-x. Zhao, Q.-h. Cai, and X.-z. Wang, *Gas adsorption on silicene: a theoretical study.* Computational Materials Science, 2014. **87**: p. 218-226.

62.   Hu, W., N. Xia, X. Wu, Z. Li, and J. Yang, *Silicene as a highly sensitive molecule sensor for NH 3, NO and NO 2.* Physical Chemistry Chemical Physics, 2014. **16**(15): p. 6957-6962.

63.   Zheng, J., R.A. Barton, and D. Englund, *Broadband coherent absorption in chirped-planar-dielectric cavities for 2D-material-based photovoltaics and photodetectors.* ACS Photonics, 2014. **1**(9): p. 768-774.

64.   刘生忠, *Agx@ WO3 core—shell nanostructure for LSP enhanced chemical sensors. Scientific.* 2015.

65.   Yang, C., F. Xiao, J. Wang, and X. Su, *3D flower-and 2D sheet-like CuO nanostructures: microwave-assisted synthesis and application in gas sensors.* Sensors and Actuators B: Chemical, 2015. **207**: p. 177-185.

66.   Mariammal, R., K. Ramachandran, G. Kalaiselvan, S. Arumugam, B. Renganathan, and D. Sastikumar, *Effect of magnetism on the ethanol sensitivity of undoped and Mn-doped CuO nanoflakes.* Applied Surface Science, 2013. **270**: p. 545-552.

67.   Chen, P., K. Xu, X. Li, Y. Guo, D. Zhou, J. Zhao, X. Wu, C. Wu, and Y. Xie, *Ultrathin nanosheets of feroxyhyte: a new two-dimensional material with robust ferromagnetic behavior.* Chemical Science, 2014. **5**(6): p. 2251-2255.

68.   Tang, J., D. Tang, R. Niessner, G. Chen, and D. Knopp, *Magneto-controlled graphene immunosensing platform for simultaneous multiplexed electrochemical immunoassay using distinguishable signal tags.* Analytical chemistry, 2011. **83**(13): p. 5407-5414.

69.   Hernandez, F.J. and V.C. Ozalp, *Graphene and other nanomaterial-based electrochemical aptasensors.* Biosensors, 2012. **2**(1): p. 1-14.

70.   Cao, X., Y. Ye, and S. Liu, *Gold nanoparticle-based signal amplification for biosensing.* Analytical biochemistry, 2011. **417**(1): p. 1-16.

71.   Zhao, C. and D. Wu, *Rapid detection assay for the molecular imprinting of gossypol using a two-layer PMAA/SiO 2 bulk structure with a piezoelectric imprinting sensor.* Sensors and Actuators B: Chemical, 2013. **181**: p. 104-113.

72.   Wang, Z., C. Zhao, T. Han, Y. Zhang, S. Liu, T. Fei, G. Lu, and T. Zhang, *High-performance reduced graphene oxide-based room-temperature NO 2 sensors: A combined surface modification of SnO 2 nanoparticles and nitrogen doping approach.* Sensors and Actuators B: Chemical, 2017. **242**: p. 269-279.

73. Berahman, M. and M. Sheikhi, *Hydrogen sulfide gas sensor based on decorated zigzag graphene nanoribbon with copper.* Sensors and Actuators B: Chemical, 2015. **219**: p. 338-345.

74. Cheran, L.-E., A. Cheran, and M. Thompson, *Biomimicry and Materials in Medicine.* 2014.

75. Dan, Y., Y. Lu, N.J. Kybert, Z. Luo, and A.C. Johnson, *Intrinsic response of graphene vapor sensors.* Nano letters, 2009. **9**(4): p. 1472-1475.

76. Jung, J.H., D.S. Cheon, F. Liu, K.B. Lee, and T.S. Seo, *A graphene oxide based immuno-biosensor for pathogen detection.* Angewandte Chemie International Edition, 2010. **49**(33): p. 5708-5711.

77. Wang, L., K. Kalyanasundaram, M. Stanacevic, and P. Gouma, *Nanosensor device for breath acetone detection.* Sensor Letters, 2010. **8**(5): p. 709-712.

78. Khan, S.B., M. Faisal, M.M. Rahman, and A. Jamal, *Low-temperature growth of ZnO nanoparticles: photocatalyst and acetone sensor.* Talanta, 2011. **85**(2): p. 943-949.

79. Xu, X., Y. Chen, S. Ma, W. Li, and Y. Mao, *Excellent acetone sensor of La-doped ZnO nanofibers with unique bead-like structures.* Sensors and Actuators B: Chemical, 2015. **213**: p. 222-233.

80. Kao, K.-W., M.-C. Hsu, Y.-H. Chang, S. Gwo, and J.A. Yeh, *A sub-ppm acetone gas sensor for diabetes detection using 10 nm thick ultrathin InN FETs.* Sensors, 2012. **12**(6): p. 7157-7168.

81. Toyooka, T., S. Hiyama, and Y. Yamada, *A prototype portable breath acetone analyzer for monitoring fat loss.* Journal of breath research, 2013. **7**(3): p. 036005.

82. Rahman, M.M., S.B. Khan, A.M. Asiri, K.A. Alamry, A.A.P. Khan, A. Khan, M.A. Rub, and N. Azum, *Acetone sensor based on solvothermally prepared ZnO doped with Co3O4 nanorods.* Microchimica Acta, 2013. **180**(7-8): p. 675-685.

83. Choi, S.-J., B.-H. Jang, S.-J. Lee, B.K. Min, A. Rothschild, and I.-D. Kim, *Selective detection of acetone and hydrogen sulfide for the diagnosis of diabetes and halitosis using SnO2 nanofibers functionalized with reduced graphene oxide nanosheets.* ACS applied materials & interfaces, 2014. **6**(4): p. 2588-2597.

84. Xiao, T., X.-Y. Wang, Z.-H. Zhao, L. Li, L. Zhang, H.-C. Yao, J.-S. Wang, and Z.-J. Li, *Highly sensitive and selective acetone sensor based on C-doped WO 3 for potential diagnosis of diabetes mellitus.* Sensors and Actuators B: Chemical, 2014. **199**: p. 210-219.

85. Zhu, J., L. Xu, and J. He, *Assembly of graphene nanosheets and SiO2 nanoparticles towards transparent, antireflective, conductive, and superhydrophilic multifunctional hybrid films.* Chemistry–A European Journal, 2012. **18**(51): p. 16393-16401.

86. Pramanik, K., P. Sarkar, and D. Bhattachayay, *Estimation of Acetone in Breath Using α D-galactose for Diabetes Monitoring.*

87. Tazhmoyev, C.D., A. McGrowder, and J.M. Rawlins, *An assessment of falsely convicted type 1 diabetics in Jamaica by using the breathalyzer test.* Journal of Clinical and Diagnostic Research, 2011. **5**(3).

88. Rahman, H., S. Barua, M.U. Ahmed, S. Begum, and B. Hök. *A Case-Based Classification for Drivers' Alcohol Detection Using Physiological Signals*. in *The 3rd EAI International Conference on IoT Technologies for HealthCare HealthyIoT'16, 18 Oct 2016, VÃ¤ sterÃ¥ s, Sweden*. 2016.

89. Hlastala, M.P. and J.C. Anderson, *Alcohol breath test: gas exchange issues.* Journal of Applied Physiology, 2016. **121**(2): p. 367-375.

90. Yu, X., W. Zhang, P. Zhang, and Z. Su, *Fabrication technologies and sensing applications of graphene-based composite films: Advances and challenges.* Biosensors and Bioelectronics, 2017. **89**: p. 72-84.

91.   Paredes, J., S. Villar-Rodil, A. Martínez-Alonso, and J. Tascon, *Graphene oxide dispersions in organic solvents.* Langmuir, 2008. **24**(19): p. 10560-10564.

92.   Liang, Y.T. and M.C. Hersam, *Highly concentrated graphene solutions via polymer enhanced solvent exfoliation and iterative solvent exchange.* Journal of the American Chemical Society, 2010. **132**(50): p. 17661-17663.

93.   Behabtu, N., J.R. Lomeda, M.J. Green, A.L. Higginbotham, A. Sinitskii, D.V. Kosynkin, D. Tsentalovich, A.N.G. Parra-Vasquez, J. Schmidt, and E. Kesselman, *Spontaneous high-concentration dispersions and liquid crystals of graphene.* Nature nanotechnology, 2010. **5**(6): p. 406-411.

94.   Zhang, X., A.C. Coleman, N. Katsonis, W.R. Browne, B.J. Van Wees, and B.L. Feringa, *Dispersion of graphene in ethanol using a simple solvent exchange method.* Chemical Communications, 2010. **46**(40): p. 7539-7541.

95.   O'Neill, A., U. Khan, P.N. Nirmalraj, J. Boland, and J.N. Coleman, *Graphene dispersion and exfoliation in low boiling point solvents.* The Journal of Physical Chemistry C, 2011. **115**(13): p. 5422-5428.

96.   Xu, J., D.K. Dang, X. Liu, J.S. Chung, S.H. Hur, W.M. Choi, E.J. Kim, and P.A. Kohl, *Liquid-phase exfoliation of graphene in organic solvents with addition of naphthalene.* Journal of colloid and interface science, 2014. **418**: p. 37-42.

97.   Berger, M., *Nanotechnology: The Future is Tiny*. 2016: Royal Society of Chemistry.

98.   Yan, C., J. Wang, W. Kang, M. Cui, X. Wang, C.Y. Foo, K.J. Chee, and P.S. Lee, *Highly stretchable piezoresistive graphene–nanocellulose nanopaper for strain sensors.* Advanced materials, 2014. **26**(13): p. 2022-2027.

99.   Wang, Y., L. Wang, T. Yang, X. Li, X. Zang, M. Zhu, K. Wang, D. Wu, and H. Zhu, *Wearable and highly sensitive graphene strain sensors for human motion monitoring.* Advanced Functional Materials, 2014. **24**(29): p. 4666-4670.

100.   Jing, Z., Z. Guang-Yu, and S. Dong-Xia, *Review of graphene-based strain sensors.* Chinese Physics B, 2013. **22**(5): p. 057701.

101.   Kuila, T., S. Bose, P. Khanra, A.K. Mishra, N.H. Kim, and J.H. Lee, *Recent advances in graphene-based biosensors.* Biosensors and Bioelectronics, 2011. **26**(12): p. 4637-4648.

102.   Aguey-Zinsou, K.-F. and J.-R. Ares-Fernández, *Hydrogen in magnesium: new perspectives toward functional stores.* Energy & Environmental Science, 2010. **3**(5): p. 526-543.

103.   Ferrari, L., J. Kaufmann, F. Winnefeld, and J. Plank, *Interaction of cement model systems with superplasticizers investigated by atomic force microscopy, zeta potential, and adsorption measurements.* Journal of Colloid and Interface Science, 2010. **347**(1): p. 15-24.

104.   Kayser, H., *Ueber die Verdichtung von Gasen an Oberflächen in ihrer Abhängigkeit von Druck und Temperatur.* Annalen der Physik, 1881. **250**(11): p. 450-468.

105.   Basova, T., C. Taşaltın, A. Gürek, M. Ebeoğlu, Z. Öztürk, and V. Ahsen, *Mesomorphic phthalocyanine as chemically sensitive coatings for chemical sensors.* Sensors and Actuators B: Chemical, 2003. **96**(1): p. 70-75.

106.   Malakootian, M., A. Almasi, and H. Hossaini, *Pb and Co removal from paint industries effluent using wood ash.* International Journal of Environmental Science & Technology, 2008. **5**(2): p. 217-222.

107.   Langmuir, I., *THE CONSTITUTION AND FUNDAMENTAL PROPERTIES OF SOLIDS AND LIQUIDS. PART I. SOLIDS.* Journal of the American Chemical Society, 1916. **38**(11): p. 2221-2295.

108.   Srivastava, V., C. Weng, V. Singh, and Y. Sharma, *Adsorption of nickel ions from aqueous solutions by nano alumina: kinetic, mass transfer, and equilibrium studies.* Journal of Chemical & Engineering Data, 2011. **56**(4): p. 1414-1422.

109.   Altintas, Z., M. Gittens, A. Guerreiro, K.-A. Thompson, J. Walker, S. Piletsky, and I.E. Tothill, *Detection of waterborne viruses using high affinity molecularly imprinted polymers.* Analytical chemistry, 2015. **87**(13): p. 6801-6807.

110.   Idil, N., M. Hedström, A. Denizli, and B. Mattiasson, *Whole cell based microcontact imprinted capacitive biosensor for the detection of Escherichia coli.* Biosensors and Bioelectronics, 2017. **87**: p. 807-815.

111.   Osman, B., L. Uzun, N. Beşirli, and A. Denizli, *Microcontact imprinted surface plasmon resonance sensor for myoglobin detection.* Materials Science and Engineering: C, 2013. **33**(7): p. 3609-3614.

112.   Dibekkaya, H., Y. Saylan, F. Yılmaz, A. Derazshamshir, and A. Denizli, *Surface plasmon resonance sensors for real-time detection of cyclic citrullinated peptide antibodies.* Journal of Macromolecular Science, Part A, 2016. **53**(9): p. 585-594.

113.   Sener, G., L. Uzun, R. Say, and A. Denizli, *Use of molecular imprinted nanoparticles as biorecognition element on surface plasmon resonance sensor.* Sensors and Actuators B: Chemical, 2011. **160**(1): p. 791-799.

114.   Diltemiz, S.E., A. Denizli, A. Ersöz, and R. Say, *Molecularly imprinted ligand-exchange recognition assay of DNA by SPR system using guanosine and guanine recognition sites of DNA.* Sensors and Actuators B: Chemical, 2008. **133**(2): p. 484-488.

115.   Ren, K. and R.N. Zare, *Chemical recognition in cell-imprinted polymers.* ACS nano, 2012. **6**(5): p. 4314-4318.

116.   Wulff, G. and A. Sarhan. *Use of polymers with enzyme-analogous structures for resolution of racemates*. in *Angewandte Chemie-International Edition*. 1972. WILEY-V CH VERLAG GMBH MUHLENSTRASSE 33-34, D-13187 BERLIN, GERMANY.

117.   Saylan, Y., F. Yilmaz, E. Özgür, A. Derazshamshir, H. Yavuz, and A. Denizli, *Molecular Imprinting of Macromolecules for Sensor Applications.* Sensors, 2017. **17**(4): p. 898.

118.   Ertürk, G. and B. Mattiasson, *Molecular imprinting techniques used for the preparation of biosensors.* Sensors, 2017. **17**(2): p. 288.

119.   Song, X., J. Wang, and J. Zhu, *Effect of porogenic solvent on selective performance of molecularly imprinted polymer for quercetin.* Materials Research, 2009. **12**(3): p. 299-304.

120.   Haupt, K., *Noncovalent molecular imprinting of a synthetic polymer with the herbicide 2, 4-dichlorophenoxyacetic acid in the presence of polar protic solvents*. 1998, ACS Publications.

121.   Lika, K., M.R. Kearney, and S.A. Kooijman, *The "covariation method" for estimating the parameters of the standard Dynamic Energy Budget model II: properties and preliminary patterns.* Journal of Sea Research, 2011. **66**(4): p. 278-288.

122.   Shamsudin, S.R. *Scanning electron microscope (SEM) & how it works*. 2011 [cited 2017 05/24/2017]; Available from: http://emicroscope.blogspot.com/2011/03/scanning-electron-microscope-sem-how-it.html.

123.   Ferrante, C., A. Virga, L. Benfatto, M. Martinati, D. De Fazio, U. Sassi, C. Fasolato, A. Ott, P. Postorino, and D. Yoon, *Raman spectroscopy of graphene under ultrafast laser excitation.* arXiv preprint arXiv:1704.00186, 2017.

124.   Деева, Ю. *Laboratory Raman spectroscopy ISP NASU*. 2015 [cited 2017 05/24/2017]; Available from: https://www.slideshare.net/ssuser6938f11/laboratory-47659130.

125. Das, A., B. Chakraborty, and A. Sood, *Raman spectroscopy of graphene on different substrates and influence of defects.* Bulletin of Materials Science, 2008. **31**(3): p. 579-584.
126. Smith, B.C., *Fourier transform infrared spectroscopy.* CRC, Boca Raton, FL, 1996.
127. Zhang, X.K., E.G. Lewars, R.E. March, and J.M. Parnis, *Vibrational spectrum of the acetone-water complex: a matrix isolation FTIR and theoretical study.* The Journal of Physical Chemistry, 1993. **97**(17): p. 4320-4325.
128. Cejer, M.A., *Choosing the Optimal Source Measurement Unit Instrument for Your Test and Measurement Application*, in *Source measure unit*, Wikipedia, Editor. 2016: Wikipedia, Tektronix.
129. Thyagi, M.S., *Introduction To Semiconductor Materials And Devices*. Resistivity by Four Probe Method, ed. V.L.a.A.V. Vidyapeetham. 2008, vlab.amrita.edu: John Wiley& Sons.
130. ULVAC, *Flat Panel LCD TVs and Vacuum*, in *Vacuum Magazine*. 2016, ULVAC: ULVAC Japanese Comapny website.
131. Koenig, J. and A. Angood, *Raman spectra of poly (ethylene glycols) in solution.* Journal of Polymer Science Part A-2: Polymer Physics, 1970. **8**(10): p. 1787-1796.
132. Ullah, R. and Y. Zheng, *Raman spectroscopy of 'Bisphenol A'.* Journal of Molecular Structure, 2016. **1108**: p. 649-653.
133. Dias, N.C., P.A. Steiner, and M.C.B. Braga, *Characterization and Modification of a Clay Mineral Used in Adsorption Tests.* Journal of Minerals and Materials Characterization and Engineering, 2015. **3**(04): p. 277.
134. Han, P., H. Wong, and M. Poon, *Sensitivity and stability of porous polycrystalline silicon gas sensor.* Colloids and Surfaces A: Physicochemical and Engineering Aspects, 2001. **179**(2): p. 171-175.